Theoretical approach to the transmission coefficient of light diffracted from a luminescent rod

Bachelor Thesis

Kyla Mikaëla van den Bogaerde*

Utrecht University
Faculty of Science
Physics & Astronomy and Mathematics
Student number: 4011139
K.M.vandenBogaerde@uu.nl

Supervisors:

Dr. Dick K.G. de Boer
Principal Scientist, Photonic Materials and Devices
Philips Research

Dr. Arnout Imhof
Associate Professor, Soft Condensed Matter and Biophysics
Utrecht University

January 12, 2016

Abstract

In this thesis a simulation is described to estimate the transmission from a luminescent rod (Lumirod) with a pyramid structured diffraction grating. The aim is to optimize the transmission. A Lumirod is a rectangular phosphor cuboid that absorbs and emits light. Most of the emitted light remains captured within the Lumirod, due to its high refractive index. When transmitted from the diffraction grating on one side of the rod, the light is coupled out. This phenomena has theoretically been approached with a simulation to calculate the total transmission coefficient. For a grating constant of 500nm this coefficient is 0.312, and for a 2µm period the total transmission 0.349 is obtained. A greater variety of diffraction structures should be modeled to make a solid statement about the structure that optimizes the transmission.

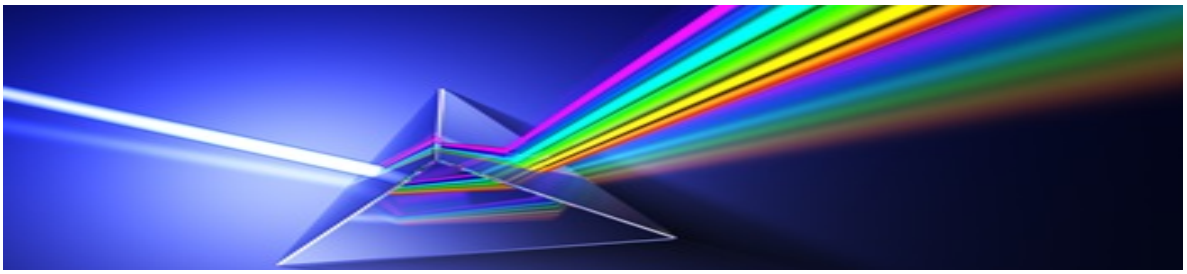

*This paper has been written as thesis for both bachelors Physics & Astronomy and Mathematics at Philips Research.

Preface

This thesis has been written as part of my graduation at Utrecht University. During the past six months I have participated in a research project at Philips Research. This experience has given me the chance to develop my practical skills, by applying theoretical knowledge to a specific subject. Since my studies are rather theoretical, applying these theories in a practical way for further research has been extremely interesting and instructive to me.
Furthermore this internship has challenged me to develop my software programming techniques. Developing models at the edge of the possibilities of existing software programs has offered me lots of practice in the programming of codes.
Most of all, I have had the opportunity to get a taste of Research and Development, a field in which I might continue after completing a master. I am grateful to many whom have made it possible for me to achieve this experience.
I would like to thank all project members and other colleagues within the department. Especially my supervisor Dick de Boer, who has thought me lots of new physical applications of theories and has made corrections in my work, I would like to pay tribute to. I would not have been able to achieve this thesis without his guidance. In addition, I want to thank project leader Henri Jagt for giving me the possibility to participate in his project group and guiding the progress of this research. At last, I would like to thank my supervisor of Utrecht University, Arnout Imhof, for advising me, giving structure and making corrections to my thesis.

Contents

1 Introduction

Nowadays, LEDs are becoming the preferred technique of illumination within many applications. Only few applications exist where gas-discharge lamps are more often applied than LEDs. Projection is an example of such an application where these lamps are still preferred, due to their ability to provide a small source with high brightness. The short life time of these gas-discharge lamps is a major disadvantage. However, it is not possible to implement LEDs in an application as projection. Multiple LEDs may combine to one bright source, however they can never combine the light in a small bright area, with low angular divergence. Therefore the power per surface area per angle of LEDs is not suitable for projection [1].

To accomplish that LEDs can be implemented for projection, a new mechanism to convert light in a LED projector is being developed at Philips. The current technique is a so called Lumirod with Compound Parabolic Concentrator (CPC) shown in figure 1B [2]. The Lumirod is a rectangular cuboid with size 1.2 x 1.9 x 52 mm and high refractive index, approximately 1.83. The Lumirod consists of a material similar to Cerium (III)-doped Yttrium Aluminum Garnet, a phosphor that absorbs light with a wavelength around 450nm. The light from the LEDs is absorbed by the Lumirod material and emitted at a longer wavelength, approximately 550nm, reestablishing the state of lowest energy. The absorption spectrum and emission spectrum of the phosphor are shown in figure 2.

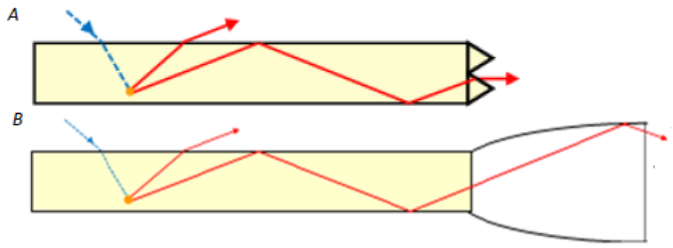

Figure 1: Schematic two dimensional view of the Lumirod with pyramid structure (A) and with the CPC (B) [2].

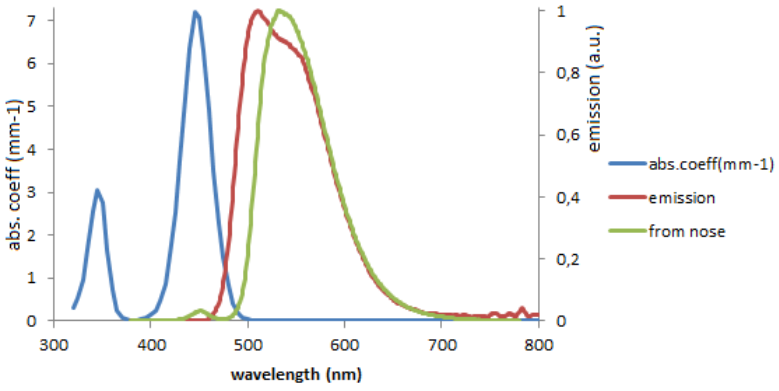

Figure 2: The absorption spectrum and emission spectrum of the phosphor. The green line represents the shifted red emission spectrum that refracts out of the Lumirod.

Due to the high refractive index of the Lumirod most of the emitted light remains captured within the rod. To extract the captured light from the Lumirod the CPC, a parabolic cap with in approximation the same refractive index as the rod, is placed on the smallest surface of the rod. The shape of the CPC is such that it bends most of the light toward its opposite site in a way that the light strikes the side with an angle of incidence smaller than the angle of total internal reflection. This causes the light to leave the rod with low angular divergence, which makes it possible to use the emitted light in a LED projector.

However, this mechanism with the CPC has some disadvantages. The CPC enlarges the area from which light is emitted, to name one. That is why a different method to extract light from the Lumirod is being developed. Instead of placing a CPC on the smallest surface of the rod, creating a nanostructure on that surface can diffract the light such that it leaves the rod as well. Figure 1A shows a schematic view of this concept.

Anne Souren has done practical experiments for research group Photonic Materials and Devices of Philips Research to test this insight [2]. She has focused on creating pyramid structured gratings on the rod, with a grating constant of 2μm, a height of 1μm and refractive indices in a range of 1.7 to 2, by varying the substances to make the pyramid grated layer. Furthermore she has tested the efficiency of these structures. Some examples of the grating structures made are shown in figure 3. These figures show that the structures made, can deviate from a perfect pyramid structured grating, and are only approximately pyramids of height 1μm and width 2μm.

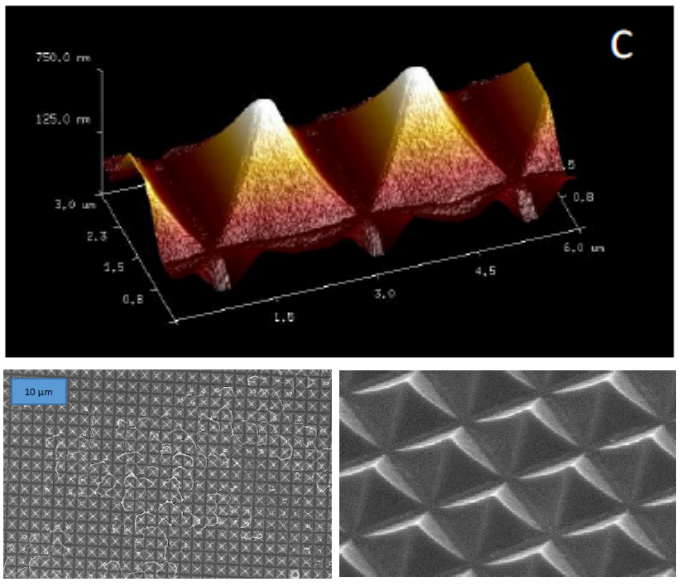

Figure 3: Examples of experimentally created and tested structures on the rod. These pyramid microstructures are created from a titanium oxide layer [2].

The composition of substances for which optical experiments have been done, has a refractive index of 1.936. By experimentally testing the efficiency of this structure, the gain if compared to the fraction of light extracted from an unstructured rod is found to be between 1.55 and 1.74. Since these numbers appear to be higher than initially expected, this theoretical research has been started to clarify the results.

The gain is the ratio between the total transmission coefficient of the Lumirod with a grating structure and an unstructured Lumirod. For the experimentally obtained transmission coefficients, the total intensity of light extracted from the nose of the Lumirod is measured. This is divided by an approximation of the total intensity of light at the nose of the rod. To obtain this approximation,

measurements have been done at Philips Research to calculate the intensity of the light emitted within the Lumirod. This total emitted intensity has been used as the total intensity at the nose of the rod, for the calculation of the transmission coefficients. In approximation this emitted intensity within the rod is the total intensity at the nose of the rod, except that not all light emitted in the Lumirod reaches the nose.

Within this thesis a simulation of the Lumirod with a pyramid structured grating, of period 2μm and height 1μm, will be modeled. To approximate the Lumirod we will simulate an infinite plane with a pyramid structured grating of width 2μm and height 1μm. Since the composition of substances of the structure that best reflects a pyramid structured grating with this geometry has a refractive index of 1.93, this number will be used for the modeled pyramids. Furthermore, a plane wave of wavelength 550nm will travel from a substrate with refractive index 1.83, through the pyramid grated plane, to a superstrate of refractive index 1. In this way the substrate will resemble the Lumirod that emits light with a wavelength of 550nm and the superstrate will be air. Although in reality light is emitted in a broader wavelength range, it is expected to obtain a good impression by doing simulations for 550 nm.
Finally, since not all angles are present at the end of the Lumirod (section 3), we will only take into account angles of incidence within the range $[-57^\circ, 57^\circ]$.

Finally, the transmission coefficients of an s-polarized and p-polarized plane wave will be calculated, to obtain the gain of the Lumirod if compared to an unstructured rod, after which we compare this theoretical calculated gain with the experimentally obtained gain. Hereby we assume the light emitted within the Lumirod is for one half p-polarized and the other half is s-polarized.

To further explore the effect of different grating structures on the diffractive outcoupling of light from the Lumirod, the same model, with instead a period of 500nm and the same geometrical proportions, is simulated. Again the transmission will be explored.

2 Theoretical background

2.1 Maxwell's equations

Maxwell's equations are a set of differential equations that describe how electric and magnetic fields are influenced by each other or by currents and charges. They are the principal building blocks of electrodynamics in the same way that Newton's laws are for classical mechanics. Many theories within this field of physics have been derived from the Maxwell equations [3], [4], [5].
Maxwell's equations in matter in there most general differential form are:

$$\nabla \cdot \boldsymbol{D} = \rho_f \tag{1}$$

$$\nabla \cdot \boldsymbol{B} = 0 \tag{2}$$

$$\nabla \times \boldsymbol{E} = -\frac{\partial \boldsymbol{B}}{\partial t} \tag{3}$$

$$\nabla \times \boldsymbol{H} = \boldsymbol{J}_f + \frac{\partial \boldsymbol{D}}{\partial t} \tag{4}$$

Here $\boldsymbol{E}$ is the electric field, $\boldsymbol{B}$ the magnetic field, $\boldsymbol{D}$ the electric displacement, $\boldsymbol{H}$ the auxiliary magnetic field, ρ_f the density of free charge and $\boldsymbol{J}_f$ the current of free charge with

$$\boldsymbol{D} = \epsilon \boldsymbol{E}, \qquad \boldsymbol{H} = \frac{1}{\mu}\boldsymbol{B}.$$

and $\epsilon = \epsilon_0(1 + \chi_e)$ the electric permittivity, $\mu = \mu_0(1 + \chi_m)$ the magnetic permeability, χ_e and χ_m the electric respectively magnetic susceptibility [6], [7], [8].
Solving the Maxwell equations provides the electric and magnetic field everywhere through space. Hence in this project, by solving Maxwell's equations with the proper boundary conditions, one can obtain the intensities of light for every point in space.

2.2 Fresnel Equations

The Fresnel Equations follow from the Maxwell equations [9], [4]. When light travels from one medium to another medium with a different refraction index, both refraction and reflection may occur at boundary between the media. The Fresnel Equations provide the fractions of light being transmitted and reflected, as well as the phase shift of the reflected light.
This theory finds its foundation in the Maxwell equations, assuming both media are homogeneous and the interface is flat. The space in which the light travels is assumed to be semi-infinite. Furthermore the light is described as a plane wave.

The Fresnel equations read

$$
\begin{aligned}
R_s &= \left| \frac{n_{in}\cos(\theta_{in}) - n_{out}\sqrt{1-\left(\frac{n_{in}}{n_{out}}\sin(\theta_{in})\right)^2}}{n_{in}\cos(\theta_{in}) + n_{out}\sqrt{1-\left(\frac{n_{in}}{n_{out}}\sin(\theta_{in})\right)^2}} \right|^2 \\
R_p &= \left| \frac{n_{in}\sqrt{1-\left(\frac{n_{in}}{n_{out}}\sin(\theta_{in})\right)^2} - n_{out}\cos(\theta_{in})}{n_{in}\sqrt{1-\left(\frac{n_{in}}{n_{out}}\sin(\theta_{in})\right)^2} + n_{out}\cos(\theta_{in})} \right|^2 \\
T_s &= 1 - R_s \\
T_p &= 1 - R_p,
\end{aligned}
$$

for which holds

$$
\begin{aligned}
R &= \frac{R_s + R_p}{2} \\
T &= \frac{T_s + T_p}{2}.
\end{aligned}
$$

Here θ_{in} is the angle of incidence, n_{in} and n_{out} are the refractive index of the substrate and superstrate respectively. Furthermore R_s, R_p are the reflection coefficients in s-polarization and p-polarization respectively, with R the total reflection coefficient. Analog to this is the transmission coefficient T. The equality $T + R = 1$ always holds.

2.3 Conservation of the wave vector

Crystal momentum is defined

$$\vec{P}_{crystal} \equiv \hbar\vec{k},$$

with $\hbar$ the reduced Planck's constant and $\vec{k}$ the wave vector (in our case of electromagnetic radiation) in the lattice [10].

While regular momentum in general is completely conserved, it follows from Maxwell's equations that crystal momentum is only conserved to within a lattice vector. This means the wave vector can always be written

$$\vec{k}' = \vec{k} + \vec{G}, \tag{5}$$

with $\vec{G}$ an arbitrary reciprocal lattice vector. The reason for this is the fact that the lattice symmetry is discrete in stead of continuous. With this conservation of the wave vector we will derive equations of diffraction from a simple cubic lattice.
Since the pyramid structure of this research has a square base, the diffraction from the structure can be compared to diffraction from a plane in a simple cubic lattice.

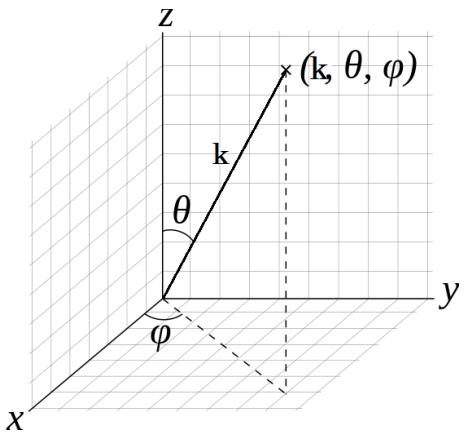

Figure 4: Wave vector in spherical coordinates.

We will write equation 5 as

$$\vec{k}_{out} = \vec{k}_{in} + \vec{G}. \tag{6}$$

From figure 4 it follows that the wave vector can be written

$$\vec{k} = ||\vec{k}|| \begin{pmatrix} \sin(\theta)\ \cos(\phi) \\ \sin(\theta)\ \sin(\phi) \\ \cos(\theta) \end{pmatrix}, \tag{7}$$

using $||\cdot||$ to denote the length of a vector [11].
To write equation 6 componentwise, the reciprocal lattice vector will be written as an arbitrary linear combination of the basis vectors in the reciprocal lattice space

$$\vec{G} = m_1\vec{a}_1^* + m_2\vec{a}_2^* + m_3\vec{a}_3^*. \tag{8}$$

Here $\vec{a}_i^*$ denotes the ith reciprocal primitive vector of the reciprocal lattice space and $m_i \in \mathbb{Z}\ \ \forall i \in \{1,2,3\}$ an arbitrary integer [12]. Given $(\vec{a}_1, \vec{a}_2, \vec{a}_3)$ the three primitive vectors for an infinite lattice space, the ith reciprocal primitive vector is defined

$$\vec{a}_i^* = 2\pi\ \frac{\vec{a}_j \times \vec{a}_k}{\vec{a}_i \cdot (\vec{a}_j \times \vec{a}_k)}\ ,$$

where i, j, k cyclic permute [13].
A simple orthorhombic Bravais lattice is a simple cubic lattice stretched along two of its base directions, hence resulting in a rectangular prism [14], [15]. It follows that for a simple orthorhombic Bravais lattice space with lattice constants d_x, d_y, d_z, respectively in the x, y and z direction, the reciprocal primitive vectors are given by

$$\vec{a}_1^* = \frac{2\pi}{d_x}\hat{x}, \quad \vec{a}_2^* = \frac{2\pi}{d_y}\hat{y}, \quad \vec{a}_3^* = \frac{2\pi}{d_z}\hat{z}. \tag{9}$$

From equations 6 , 7 , 8 , 9 and the fact that $||\vec{k}|| = \frac{2\pi}{\lambda} = \frac{2\pi \cdot n}{\lambda_0}$, with n the refraction index of the medium and λ_0 the wavelength in vacuum, we find the three equations describing diffraction from a simple orthorhombic Bravais lattice

$$n_{out} \begin{pmatrix} \sin(\theta_{out})\ \cos(\phi_{out}) \\ \sin(\theta_{out})\ \sin(\phi_{out}) \\ \cos(\theta_{out}) \end{pmatrix} = n_{in} \begin{pmatrix} \sin(\theta_{in})\ \cos(\phi_{in}) \\ \sin(\theta_{in})\ \sin(\phi_{in}) \\ \cos(\theta_{in}) \end{pmatrix} + \lambda_0 \begin{pmatrix} \frac{m_x}{d_x} \\ \frac{m_y}{d_y} \\ \frac{m_z}{d_z} \end{pmatrix}. \tag{10}$$

When a plane wave reaches the pyramid structured grating of the Lumirod the diffraction of light is equivalent to that from a two-dimensional square lattice with lattice constant d. Hence equation 10 with lattice spacing $d_x = d_y = d$ and $m_z = 0$, since we take two dimensions into account, describes the diffraction of light from the Lumirod.

2.4 Snell's law

Snell's law follows from the three equations describing ray tracing of diffraction from a simple cubic lattice (equation 10) with lattice spacing d ($d_x = d_y = d_z = d$) in the plane of incidence ($\phi_{in} = \phi_{out}$) for the zeroth order ($m_x = m_y = m_z = 0$) (figure 5)

$$n_{in} \sin(\theta_{in}) = n_{out} \sin(\theta_{out}). \tag{11}$$

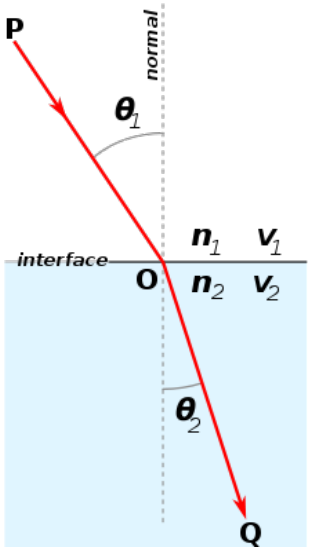

Figure 5: Refraction of light on an interface between two media [16]. Here θ_1 and θ_2 represent θ_{in} and θ_{out} respectively. The same holds for the refractive indices n.

2.5 Bragg's law

As another application of equation 10, we discuss Bragg's law [12], [17]. Bragg's law describes the angles for coherent and incoherent scattering from a crystal lattice. It can be derived from the conservation of the wave vector for a simple cubic lattice (equation 10) with lattice spacing d ($d_x = d_y = d_z = d$).
As shown in figure 6 the diffraction takes place in the plane of incidence so $\phi_{in} = \phi_{out}$. Furthermore the reciprocal lattice vector is given by $\vec{G} = m_x\vec{a}_x^* + m_y\vec{a}_y^* + m_z\vec{a}_z^*$ with $m_x = 0, m_y = 0, m_z \in \mathbb{Z}$.

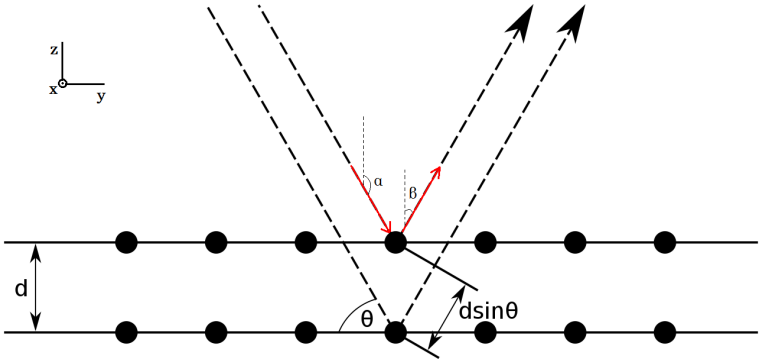

Figure 6: Bragg diffraction from a simple cubic lattice.

For the angle of incidence with the z-axis holds $\alpha = 90° + \theta$, for the angle of reflection $\beta = 90° - \theta$. Since the incoming wave vector and the outgoing wave vector travel through the same medium $n_{in} = n_{out}$. Putting all together with equation 10 three equations follow

$$n \begin{pmatrix} \sin(90° - \theta)\ \cos(\phi) \\ \sin(90° - \theta)\ \sin(\phi) \\ \cos(90° - \theta) \end{pmatrix} = n \begin{pmatrix} \sin(90° + \theta)\ \cos(\phi) \\ \sin(90° + \theta)\ \sin(\phi) \\ \cos(90° + \theta) \end{pmatrix} + \frac{\lambda_0}{d} \begin{pmatrix} 0 \\ 0 \\ m_z \end{pmatrix}$$

from which the equations for the x- and y-component are trivial.
Using that $\lambda = \frac{\lambda_0}{n}$ and $\cos(90° - x) = \sin(x)$ Bragg's law follows from the equation for the z-component

$$2d \sin(\theta) = m_z \lambda.$$

2.6 Floquet theory

To solve Maxwell's equations on an infinite periodic domain it can be convenient to apply Floquet theory, among physicists often better known as Bloch's theory. Bloch's theory is the analogous result in solid-state physics. Floquet's theorem is an important mathematical foundation for Rigorous coupled wave analysis. Furthermore, in this research, it is applied in the simulation modeled with COMSOL.

Floquet's theorem states that a solution of a periodic system $\dot{x} = A(t)x$ (i.e. $A(t)$ a p-periodic matrix) can be written $\Phi(t) = P(t)e^{Bt}$, whereas $P(t)$ a periodic matrix with the same period p as $A(t)$ [18]. From this it follows that $\Phi(t + np)$ is a solution for all n, with n an integer. Whenever the solution of the system is written in this form, the solution can be constructed given any initial conditions for infinite repetitions. Since the domain is periodic over an infinite space, especially this last property is convenient.

The exact Floquet theorem with proof are written below for completeness.

Definition 2.1. Fundamental matrix
A non-singular matrix solution $F(t)$ of the differential equation

$$\frac{dF(t)}{dt} = A(t)F(t)$$

is called a fundamental matrix [19].

Floquet's theorem states the following:

Theorem 2.1. *Floquet Theorem*
If $\Phi(t)$ is a fundamental matrix solution of the system

$$\dot{x} = A(t)x,$$

with $A(t)$ a time dependent periodic matrix with period p, then $\Phi(t + p)$ is also a fundamental matrix solution.
Moreover $\Phi(t)$ can be written

$$\Phi(t) = P(t)e^{Bt},$$

in which $P(t)$ an invertible p-periodic matrix and B a matrix.

Remark. Even though $A(t)$ is a periodic matrix, $\Phi(t)$ need not to be periodic.

Proof. Given a system

$$\dot{x} = A(t)x,$$

with $A(t)$ a time dependent p-periodic matrix. Define $\Psi(t) = \Phi(t + p)$, with $\Phi(t)$ a fundamental matrix of the system. Since $\Phi(t)$ is invertible $\forall t \in \mathbb{R}$, $\Phi(t + p)$ is invertible, hence $\Psi(t)$ is non-singular. Furthermore

$$\dot{\Psi}(t) = \dot{\Phi}(t + p) = A(t + p)\Phi(t + p) = A(t)\Phi(t + p) = A(t)\Psi(t)$$

which states that $\Psi(t)$ is a matrix solution of the system [20]. Therefore $\Psi(t)$ is a fundamental matrix.
Define the matrix $B(t) = \Phi^{-1}(t)\Psi(t)$. It follows from

$$B(t)\Psi^{-1}(t)\Phi(t) = \left(\Phi^{-1}(t)\Psi(t)\right)\left(\Psi^{-1}(t)\Phi(t)\right) = \mathbb{I},$$

that $B(t)$ is a non-singular matrix.

Define $\beta(t) = \Phi(t)B_0$ with $B_0 = B(t_0)$. For the same reason that $B(t)$ is invertible, $\beta(t)$ is invertible. And since

$$\dot{\beta}(t) = \dot{\Phi}(t)B_0 = A(t)\Phi(t)B_0 = A(t)\beta(t),$$

$\beta(t)$ is a fundamental matrix of the system.

Evaluating both $\Psi(t)$ and $\beta(t)$ at time $t = t_0$ gives

$$\Psi(t_0) = \Phi(t_0)B(t_0) = \Phi(t_0)B_0 = \beta(t_0).$$

By uniqueness of the solution for a differential field, it follows that $\Psi(t) = \beta(t) \quad \forall\ t \in \mathbb{R}$. Hence $\Phi(t+p) = \Phi(t)B_0$ with B_0 a non-singular constant matrix.

Since every invertible $n \times n$ matrix can be expressed as e^C for some $C \in M_n(\mathbb{C})$, we write $B_0 = e^{Dp}$ where D is some constant matrix [21], [22]. Define $P(t) = \Phi(t)e^{-Dt}$ an invertible matrix, since $\Phi(t)$ and B_0 are non-singular, so that $\Phi(t) = P(t)e^{Dt}$.
Then

$$\begin{aligned} P(t+p) &= \Phi(t+p)e^{-D(t+p)} = \Phi(t)B_0e^{-D(t+p)} = \Phi(t)e^{Dp}e^{-D(t+p)} = \Phi(t)e^{D(p-(t+p))} = \Phi(t)e^{-Dt} \\ &= P(t). \end{aligned}$$

Therefore $P(t)$ is a p-periodic matrix. □

2.7 Modeling methods

The three modeling methods illustrated in this chapter are the main methods applied in software programs for solving Maxwell's equations. In this research the last two are used.

2.7.1 Finite difference time domain

Finite difference time domain (FDTD) is a numerical technique used to model electrodynamic simulations. It can cover a wide frequency range and treat nonlinear material properties in a natural way. Finite difference time domain starts from the Maxwell equations (equation 1) to analyze the time evolution of electromagnetic fields.
Specifically Ampere's law and Faraday's law show that the change in time of the electric field is dependent on the change of the magnetic field in space, and vice versa. Therefore Finite difference time domain is based on the relation that, at any point x_0 in space, the new value in time of the electric field depends on the previous value in time of the electric field and the curl of the local distribution about x_0 of the magnetic field in space. Even so at any point x_0 in space, the new value in time of the magnetic field depends on the previous value in time of the magnetic field and the curl of the local distribution about x_0 of the electric field in space.

To perform calculations using these relations, Finite difference time domain is based on one of the most basic mathematical approximations, namely finite differences [23]. In the approximation $\delta << 1$ a partial differential can be discretized in a central-difference approximation

$$\frac{\partial f(x)}{\partial x}|_{x=x_0} \approx \frac{f(x_0+\delta) - f(x_0-\delta)}{2\delta}.$$

With this approximation Finite difference time domain can be summarized in five principal steps:

- Discretize time and space by replacing all (partial) derivatives in Ampere's and Faraday's law with a central-difference approximation.
- Rewrite the obtained discretized equations, such that the future (unknown) time step of both the electric and magnetic field is written as a function of the previous time step of the electric respectively magnetic field and the curl of the magnetic respectively electric field of the previous time step.
- Evaluate the electric field one step in time, this future step now becomes the previous step since it has just become known.
- Evaluate the magnetic field one step in time, in the same way as the electric field, this magnetic field now becomes the previous step.
- Repeat the previous two steps over the desired time to evaluate both fields for.

2.7.2 Finite element method

The Finite Element Method (FEM) is a numerical technique to approximate the solution of a set of partial differential equations constricted to the boundary conditions of the problem domain. The idea of the technique is to subdivide the problem domain into many simpler parts, named finite elements, in which the parameters describing the domain properties can be considered constant [24]. By solving the differential equations on these finite elements and connecting them to the solution of the differential equations on their neighbor elements, an approximation of the solution on the complex equations of the whole problem domain is made.

The finite element method can be formulated using the weighted residual method [25]. Introducing the basic principle of this method, we consider a general partial differential equation on the solution domain Ω

$$\mathscr{L}\phi = f. \tag{12}$$

Here f represents a given function, ϕ is the function we will solve for and $\mathscr{L}$ the differential operator.
The first step is to subdivide the solution domain into N smaller subdomains, such that the function to solve for can be written as a expansion of basis functions on the subdomains

$$\phi = \sum_{i=0}^{N} c_i v_i. \tag{13}$$

These subdomains are the finite elements. The basis is given by the set $\{v_i\}$ for (i=1,2,...,N). The coefficients are denoted by $\{c_i\}$, they represent the value of ϕ at the boundary between the i^{th} and $i + 1^{th}$ subdomain.
Substituting expansion 13 in equation 12 and integrating over the entire solution domain with a given weighted function w_j, yields

$$\int_\Omega w_j \mathscr{L} \left(\sum_{i=1}^{N} c_i v_i \right) d\Omega = \int_\Omega w_j f d\Omega. \tag{14}$$

In general the most popular choice for the weighted function is $w_j = v_j$, therefor equation 14 becomes

$$\sum_{i=1}^{N} c_i \int_\Omega v_j \mathscr{L}(v_i) d\Omega = \int_\Omega v_j f d\Omega \qquad j = 1, 2, ..., N.$$

This expression defines a set of N linear algebraic equations that, given the initial and boundary conditions, can be solved for $\{c_i\}$. In this way, the solution ϕ of equation 12 is obtained.

2.7.3 Rigorous coupled wave analysis

Rigorous coupled wave analysis (RCWA) is a computational method used for electromagnetics. It is most typically applied to solve scattering from periodic dielectric structures. The method is based on Fourier transformations. In the modeled simulation of the system, devices and fields are represented as an expansion of principal wave functions of the system, i.e. a sum of spatial harmonics [26].
Floquet's theorem (section 2.6) has an important role in Rigorous coupled wave analysis. It makes use of the fact that solutions of periodic differential equations can be expanded with Floquet functions (equation 2.1). (Often referred to, in solid state physics, as Bloch waves.) Since the simulation of the Lumirod is done in an infinite plane with a pyramid structured grating, the Maxwell equations are solved on a periodic domain. Hence the solutions of these periodic differential equations can be written as Floquet functions.

To do a model calculation, a device is divided into layers [27]. All layers are uniform in one of three spatial directions x,y or z.
For oblique or curved devices, or devices with for instance a dielectric permittivity graded (i.e. non homogeneous) along the uniform direction of the layers, the structure of the device is built up in a staircase approximation.
In the simulation of the Lumirod, the curved device that is divided into layers, built up in a staircase approximation, corresponds with the pyramids of the grating structure. These layers are uniform in the direction from the base of the pyramids to the top. In figure 7 a two dimensional view of this pyramid structure, based on layers in a staircase approximation, is shown.

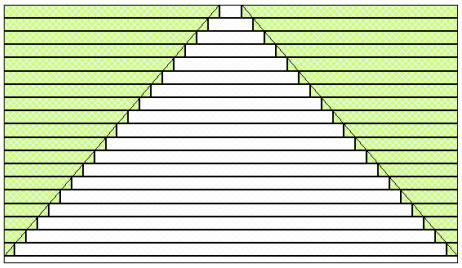

Figure 7: Two dimensional front view of a staircase approximation of a pyramid, based on layers.

The electromagnetic harmonics are calculated in all the layers individually, after which they are propagated through the layers analytically. By matching the boundary conditions at all interfaces between the layers and at the borders of the device, the electric modes can be solved uniquely. The boundary condition at the interface where the plane wave reaches the device is determined by the wave vector of this incident plane wave in the periodic dielectric medium.

3 Modeling

In this research our goal is to model the nanostructure on the rod as an infinite plane of pyramids to get an insight of the influence of transmitted and reflected diffraction orders on the transmitted intensity. The refractive index of the Lumirod is 1.83, it emits light with a wavelength around 550nm and the nanostructure on the rod has an index of approximately 1.936. Hence we will simulate in our model such that a plane wave of wavelength 550nm travels from a superstrate of refractive index 1.83 through the infinite plane with pyramid structure of index 1.936 to a substrate of index 1, in approximation the refractive index of air.
One unit cell (i.e. one period) of the geometrical structure of the modeled pyramids is shown in figure 8. Here d is the so called grating constant of the structure. It represents the periodicity in both the x and y direction.
Furthermore the emitted rays in the rod can include all kind of polarization directions. Therefore we will look at both a s-polarized plane wave and a p-polarized plane wave separately. These two polarizations together form a orthogonal basis for all polarizations, hence we can describe any arbitrary polarization in our rod.
We will not take into account that any energy might be absorbed in the system, neither that there are any external electrodynamic influences.

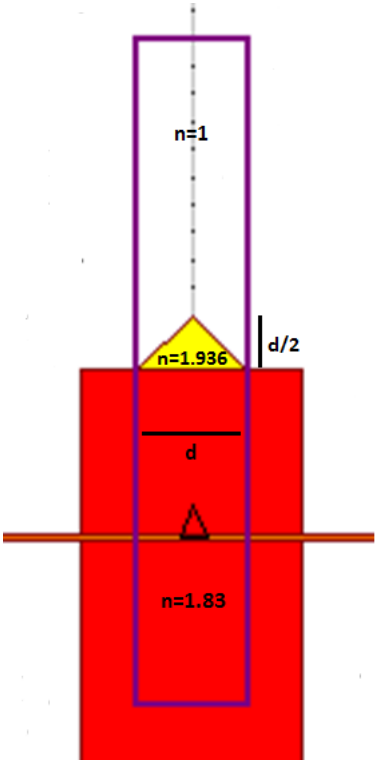

Figure 8: A two dimensional view of one unit cell of the simulated pyramid structured grating, with grating constant d.

With Snell's law (equation 11) we find the critical angle of the rod to be

$$\theta_{crit} = \arcsin(\frac{1}{1.83}) \approx 33^\circ.$$

We will do simulations for all angles of incidence, but in the evaluation of the results we will take into account that not all angles of incidence on the pyramid structure are equally likely. A ray emitted by the rod will eventually reach a side with some angle of incidence. Figure 9 shows a two-dimensional simplification of these possible ray trajectories when the absorbed beam gets emitted within the rod.

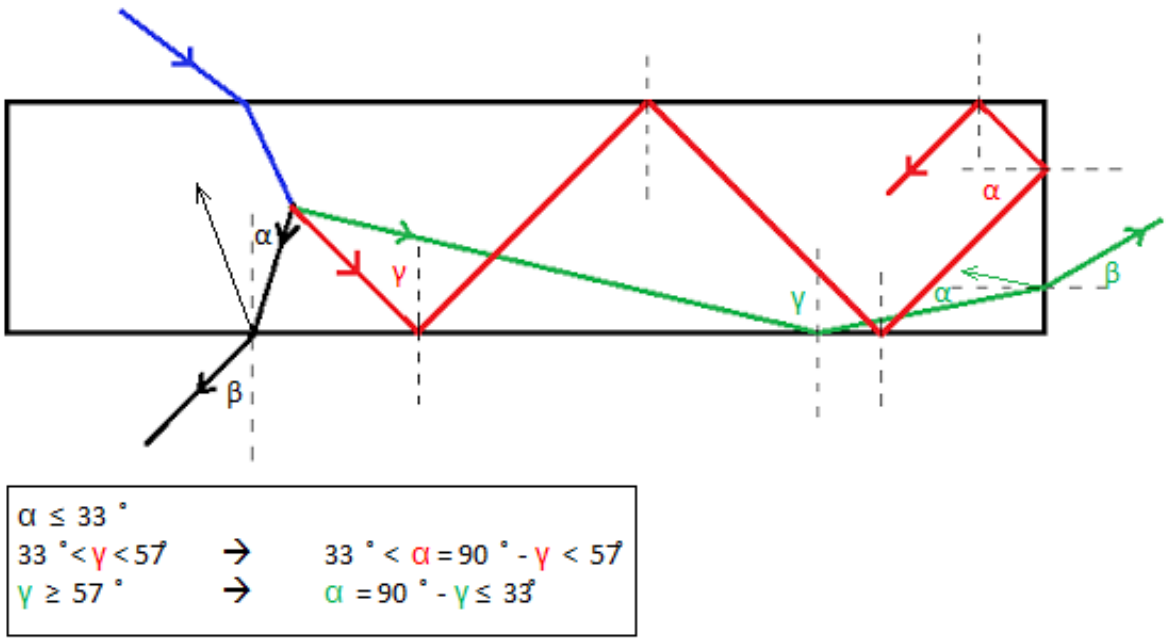

Figure 9: Ray trace trajectory inside the rod without pyramid structure. From a ray that reaches a long side of the rod with an angle of incidence $\theta_{in} \leq \theta_{crit}$ (black line) only the Fresnel reflection remains inside the rod. A ray that reaches the rod with an angle $\theta_{crit} < \theta_{in} < 90° - \theta_{crit}$ (red line), under the assumption that no energy disappears in the system, will keep on circulating within the rod for ever. Finally, a ray with an angle of incidence $\theta_{in} \geq 90° - \theta_{crit}$, when reaching a long side of the rod, (green line) will escape from the rod at the short side according to the Fresnel equations.

When the angle of incidence, at which a ray reaches a long side of the rod, is less than or equal to the critical angle of the rod, the ray is transmitted and leaves the rod with only the Fresnel reflection remaining inside the rod (black beam). We will neglect this reflected part of the ray, since $R << 1$ for angles $\theta_{in} < \theta_{crit}$. Figure 10 shows the s-polarized and p-polarized Fresnel reflections on a flat interface between the rod and the air, showing that, for $\theta_{in} < \theta_{crit}$, indeed R«1. Nevertheless the reflection is certainly not zero.

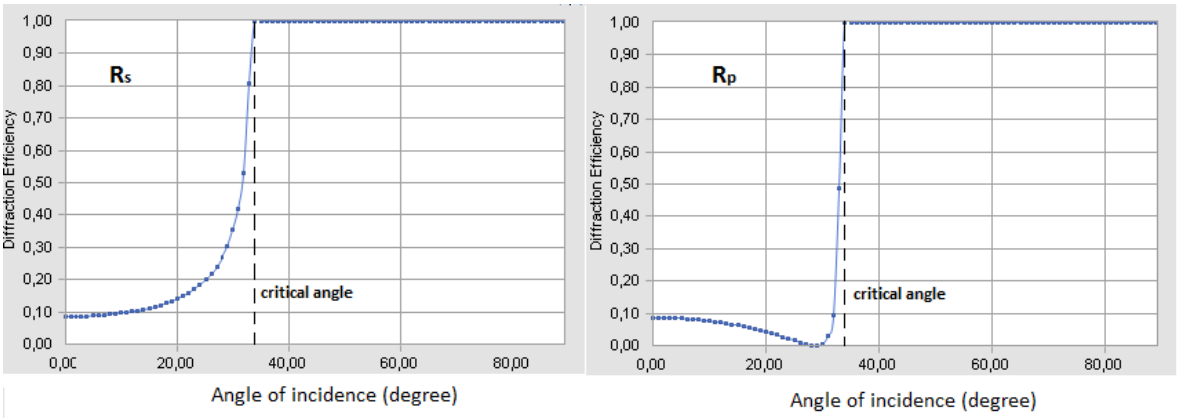

Figure 10: The s-polarized and p-polarized Fresnel reflection coefficients on a flat interface from a substrate of refraction index 1.83 to a superstrate with index 1.

The opposite holds for an angle of incidence $\theta_{crit} < \theta_{in} < 90° - \theta_{crit}$ (red beam). Such a ray is captured within the rod because it will strike every side of the rod with an angle $\theta_{crit} < \theta_{in} < 90° - \theta_{crit}$ and therefore total internal reflection of the ray occurs.
Finally if the ray reaches the long surface of the rod under an angle $\theta_{in} \geq 90° - \theta_{crit}$ the ray is internally reflected at this side. However this ray will strike the short side of the rod with an angle less then the critical angle and hence be transmitted at this surface. Again a small part of this ray remains inside the rod due to Fresnel reflection (green beam).
Summarizing the above, we find that light that indirectly (by first striking one of the four long sides of the rod) reaches the short side of the rod, strikes the short side with an angle less than $90° - \theta_{crit} \approx 57°$. Note that this holds in two dimensions, in a plane perpendicular to two sides. Skew rays can be at somewhat higher angles, but in first approximation we can limit ourselves to rays with $\theta < 57°$.

Most rays emitted in the rod will first strike one of the four large boundary surfaces, therefore reach the small side of the rod indirectly. This is due to the dimensions of the rod. The Lumirod has size 1.2 x 1.9 x 52 mm. Simple geometry shows that a light ray within the rod that directly strikes the pyramid structured surface with an angle of incidence greater than or equal to 57°, has been emitted within a distance of $\sqrt{1.2^2 + 1.9^2}\tan(57°) \approx 3.46$mm of that surface. Since 3.46mm is only a small fraction of 52mm we will neglect this contribution of light and therefore not take into account that the rays strike the pyramid structured surface direct, with an angle of incidence greater than 57°.
Therefore to calculate the efficiency of the nanostructure on the Lumirod, we will omit the angles of incidence $\theta_{in} \geq 57°$ on our infinite pyramid structured plane.
We assume the angles of incidence $\theta_{in} < 57°$ to be homogeneous.

3.1 COMSOL Multiphysics

COMSOL Multiphysics is a software program designed to model and simulate physics-based phenomena. It includes multiple user interfaces on a variety of physics theories, which together form a multiphysics simulation platform. Solving techniques that COMSOL uses to evaluate physics-based simulations are primarily based on the finite element method described in section 2.7.2. The specific interface used for this research project, Electromagnetic Waves Frequency Domain, applies the finite element method on Maxwell's equations (section 2.1) in order to solve these on the modeled simulation domain.

3.1.1 Modeling activities

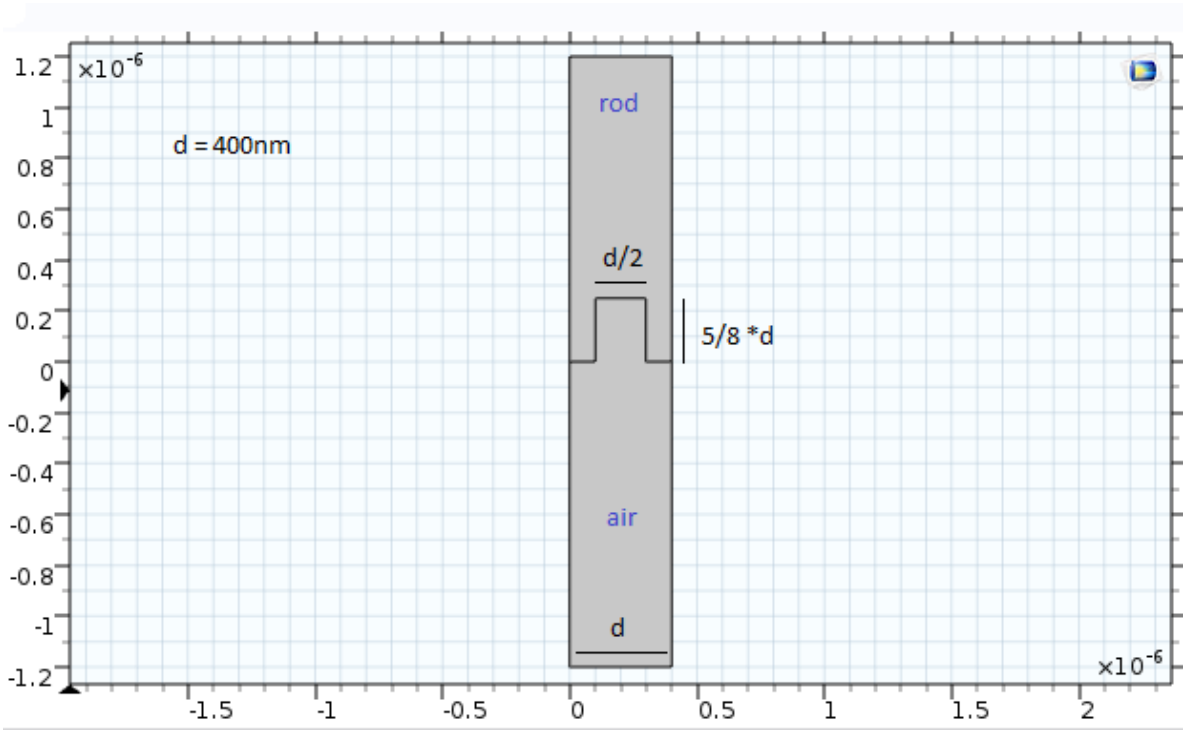

Figure 11: Two-dimensional unit cell of a rectangular grating.

One of the first simplified simulations of the rod was a two-dimensional infinite array of rectangular grating structures shown in figure 11. In this simulation a plane wave travels from a medium with refractive index 1.936 to one with index 1. The wave has wavelength 550nm in vacuum and is fully s-polarized. The wave vector is real, meaning no energy is absorbed in the system. Since we are only interested in the diffraction of a plane wave without any other electric influences, we chose that there is no external electric field. To simulate an infinite array with this grating structure Floquet periodic boundary conditions are applied to the boundaries of one unit cell.

Name	Expression	Description
n_{rod}	1.936	Refractive index rod
n_{air}	1	Refractive index air
λ_0	550nm	Wavelength in vacuum
f_0	$\frac{c}{\lambda_0}$	Frequency
d	400nm	Grating constant
θ_{in}	0	Angle of incidence
θ_{out}	$\arcsin(\frac{n_{rod}\sin(\theta in)}{n_{air}})$	Angle of refraction

Table 1: Parameters of the simulations performed with COMSOL. Here f_0 follows directly from $f = \frac{v}{\lambda}$ with v the phase velocity and c the speed of light. θ_{out} follows from Snell's law (equation 11).

To set up this simulation in COMSOL, open the Electromagnetic Waves Frequency Domain user interface and define the parameters as given in table 1. Next, first set up the geometrical structure of the diffraction grating by building a unit cell as given in figure 11 that is made with three rectangles of which two form a union together. This leaves us with two domains. To define the materials substitute the refractive index and the complex part of the wave vector for each domain. Since we do not want energy to be absorbed in the system, we choose the complex part of the wave vector to be zero. Furthermore, following the convention of the angles defined within COMSOL, we will say the upper part of the unit cell represents the rod and the lower part is air.
Now that the basics of our diffraction plane has been set up, we come to the part where we set up the electric field. Set the external electric field equal to zero. For a s-polarized plane wave, set all measurements of electric field components in the z-direction (out of plane). Finally for the electric field create two horizontal "ports" (as they are called in COMSOL), one at the top of the rod and the other one at the opposite side at the bottom of air. Port1 at the top of the rod will radiate a periodic s-polarized plane wave (meaning its electric field only has a z-component). Whereas port2 just measures the electric field in the z-direction. Substitute the refractive indices (the materials are isotropic), the frequency, the angle of incidence θ_{in} at port1 and the angle of refraction $-\theta_{in}$ at port2. The physical part of modeling the unit cell is done. By selecting Floquet periodic boundary conditions for the vertical borders of the unit cell, we turn our cell into an infinite array with this diffraction grating structure.

To finish our model we will have to subdivide the modeling domain in small parts, in such a way that COMSOL can apply the finite element method to solve Maxwell's equations in our model. To achieve this we set the mesh of an area equal to $\frac{\lambda_0}{8 \cdot n_{area}}$, the mesh of a port to $\frac{\lambda_0}{20 \cdot n_{port}}$, copy the boundaries so that the periodicity is conserved and finally create the division of the domain in triangular elements which makes our model ready for calculation. n_{area} and n_{port} are variables, corresponding to the refractive index of their particular domain, defined within COMSOL. A triangular is a 2-simplex, which simply means that any volume, regardless of shape or topology, can be meshed with it. Therefore we choose the finite elements of this calculation to be triangular elements.

3.1.2 Experience

Comparing COMSOL with GSolver In order to benchmark the results obtained with COMSOL we use GSolver to simulate exactly the same two-dimensional model (section 3.2). GSolver is specialized in solving Maxwell's equations for diffraction gratings. It therefore offers a more straightforward user interface which can be managed easier. Nevertheless in three dimensions GSolver will be inconvenient for this research, hence we will not use it for any more than a benchmark in two dimensions.

Around the 15^{th} of July, two weeks after I started, it became clear that the results obtained with COMSOL and GSolver, for the transmission and reflection coefficient as a function of the angle of incidence, did not match whenever light travels from high refractive index to low refractive index. Figures 12 and 13 show these results for the two-dimensional infinite array with a rectangular grating structure. However the other way round, when light travels from low refractive index to high refractive index the results of both software agreed perfectly. Since the results of COMSOL were not symmetric in θ and gave values for the reflection and transmission coefficient greater than one, I assumed the problem would be in the COMSOL software, hence I contacted COMSOL for the problem. Begin August after weeks of modeling slightly different diffraction gratings in both GSolver and COMSOL, comparing these to see how they differ from one another, a bug in the software of COMSOL was found in cooperation with the Dutch and Swedish COMSOL development departments.

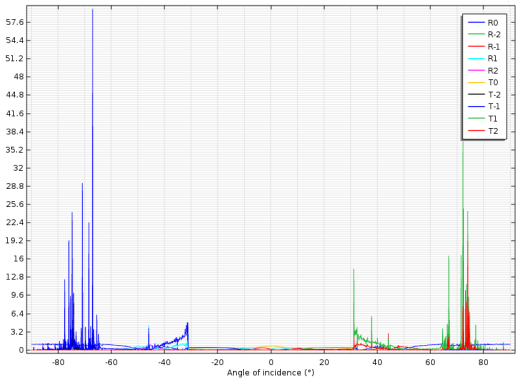

Figure 12: Transmission orders of s-polarized light on an infinite plane calculated with COMSOL while it still contains the bug. The diffraction grating is as shown in figure 11 and a grating period of 400nm. The azimuthal angle of incidence is $\phi = 0°$ and the polar angle is an element of the interval $[-90°, 90°]$.

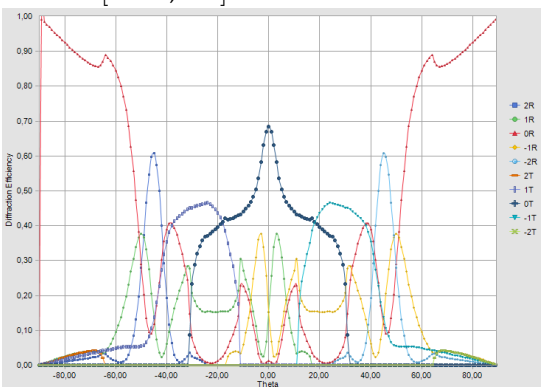

Figure 13: Repeated calculation as shown in figure 12 with the same conditions, however now calculated with GSolver.

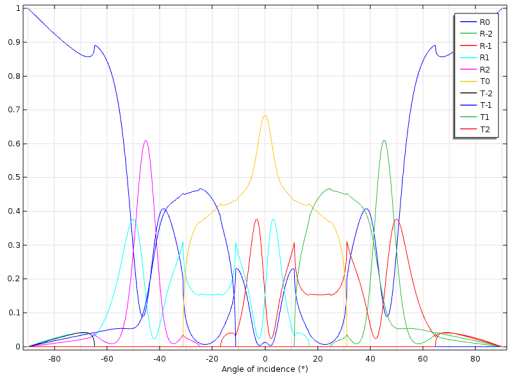

Figure 14: Repeated calculation as shown in figure 12 with the same conditions, however now calculated with COMSOL after fixing the bug.

Debugging The bug was that COMSOL's software assumed the wave vector component parallel with the port boundary is always given by:

$$k_0 \cdot n \cdot \sin(\theta),$$

where k_0 is the wave number in vacuum, n the refractive index and θ the angle of incidence or refraction. In a perfect analytic world this would be true, but in a numeric calculation this doesn't hold. Because the light travels from high to low refraction index, there is a range of angles $\theta_{in} \in [-90, -\theta_{crit}] \cup [\theta_{crit}, 90]$ for which total internal reflection of the zeroth order ($m = 0$) occurs. In this range of angles, due to numeric calculations, the angle θ becomes complex.
When COMSOL evaluates $\sin(\theta)$ for a complex angle, there will be a tiny imaginary part in the wave vector. That tiny imaginary part influences the calculations in such a way that the complex part of the wave vector blows up due to an iterative algorithm, thereby resulting in that the power was not conserved (or rather that power was obtained). Hence the transmission and reflection coefficients T and R respectively become unphysical results ($T, R >> 1$).

Correcting the software code The bug fix was to surround all sine expressions with the real(...) operator, so we only get the real part of the wave vector component parallel with the port boundaries. Unfortunately in a three-dimensional simulation this means correcting two equations per order. The amount of orders in a simulation can accumulate to about 1500 orders. Correcting these formula by hand in the programming code of COMSOL's software would easily lead to mistakes. Therefore a with java written patch was necessary to automate the correction of all diffraction orders. COMSOL was not willing to write this patch but argued that this software-update would be implemented in COMSOL5.2 available from the end of November. Therefore I started writing my own patch since I could not wait till November. COMSOL gave tips on how to adjust their software, nevertheless at the end of September the software still was not calculating properly. Eventually they finished the patch I started writing.

Late in October after just a week of working with the new written patch, it became clear that new problems appeared. The memory was too limited for the simulations I made. Furthermore the scaling of matrices in the calculation gave errors. This was due to the fact that the electric field was of much larger order of magnitude then the intensities, both turned into dimensionless quantities in order to be compared. Hence the intensities became negligible compared to the electric field, which resulted in matrices that could not influence one another. Therefore making it impossible to run the simulations. At that point I switched to RSoft and put my simulations in COMSOL aside.

3.2 GSolver

GSolver is a software program recommended for analysis of grating structures. It is designed to simulate diffractive structures in metals or dielectrics. Semiconductor manufacturing tools, including photolithographic techniques, have been built in the software.
The piecewise constant approximation is central to the mathematical solution method of GSolver, Rigorous coupled wave analysis (section 2.7.3).

3.2.1 Modeling activities

For this thesis GSolver was used as a benchmark in two dimensions for both COMSOL and RSoft. Since the desired structure to simulate is a pyramid grating, the most useful model able to be created with GSolver is a two dimensional triangle grating structure. This is the two dimensional geometric shape closest to a pyramid.
In this simulation a plane wave, of wavelength 550nm in vacuum, travels from a superstrate of refractive index 1.936, through the triangle grating with period 200nm, to a substrate of index 1. The plane wave is fully s-polarized.

To simulate this triangle grating structure in GSolver, open the first tab, named parameters, on the GSolver user interface. Define the parameters given in table 2. Choose Nanometres Units Selection and select a superstrate index of 1.936 and a substrate index of 1.

Name	Expression	Description
Vacuum wavelength	550nm	Wavelength in vacuum
Grating period	2000nm	Grating constant
Theta	0	Polar of incidence
Phi	0	Planar angle of incidence
Alpha	0	Polarization direction
Beta	0	Polarization ratio

Table 2: Parameters of the simulations created with GSolver.

After setting these parameters continue to the second tab, Graphical Editor. Draw a triangle of width 2000nm (the horizontal-axis is always one grating period) and height 1000nm. To select the refractive index 1 of the triangle, right click and go to properties, after which a selection can be made. Since GSolver automatically applies periodic boundary conditions to the structure, assumes no external electric field is present in space and no energy is absorbed in the structure, we can continue with the calculation. GSolver will calculate the piecewise constant approximation by choosing the button approximation. Moreover to implement this piecewise constant approximation in the calculation continue to the tab Listing/Run and choose Populate.

On the tab Run we can indicate which parameters we would like to vary. Since we are interested in the angle of incidence dependence of the transmission and reflection orders, we choose to vary theta for $\theta \in [-90^\circ, 90^\circ]$ in steps of one degree. Furthermore, substitute the number of desired orders to calculate for. We will choose 16 orders.
Finally, choose Run to obtain the results of the triangle structured grating just set up.
On the tab Results, the calculated data are shown. To visualize these choose chart after selecting the columns to plot.

3.3 RSoft

Synopsys' Optical Solutions Group is a developer of optical analysis and design tools. RSoft is one of these tools. It is specialized in photonic and optical network design. It is built on multiple mathematical methods, among others finite difference time domain and Rigorous coupled wave analysis. The RSoft package used for modeling doing this research is the Diffraction Module. This module relies mostly on Rigorous coupled wave analysis. This package is specialized in calculating the electromagnetic fields of light diffracted by some periodic structure.
Another module (Fullwave), which we did not use, relies on the Finite difference time domain method (section 2.7.1).

Synopsys also offers the optical ray tracing package LightTools, which is widely used within Philips. One of the advantages of RSoft is that the results can be fed into LightTools, enabling the coupling of nanoscale optics to macroscopic optics for practical applications.

3.3.1 Modeling activities

To simulate the Lumirod, we set up a model of an infinite plane with pyramid structured grating as described in the introduction of section 3. To accomplish this, first chose edit symbol and define the parameters in table 3.

Name	Expression	Description
Vacuum wavelength	550nm	Wavelength in vacuum
Grating period	2000nm	Grating constant
Theta	0	Polar of incidence
Phi	0	Planar angle of incidence
Alpha	0	Polarization direction
L	3*Period	Geometrical factor
Layers	11	Number of layers used for RCWA
M	16	Number of harmonics
Period	2	Grating constant in microns
Rod	0.83	Refractive index rod relative to the environment (air)
TiO2	0.936	Refractive index pyramid structure relative to the environment (air)

Table 3: Parameters of the simulations created with RSoft.

After defining the parameters, choose Global Settings to define how these parameters should be integrated in the model. Since the wave length of the plane wave is 550nm, substitute 0.55 for the wavelength. (Remark that microns is the unit.) The surrounding of the Lumirod is air, therefore we will simulate the model with a background refractive index of 1. Also check the box 3D, since the model is set up in three dimensions.

All definitions have been introduced, therefore the geometric structure will be generated now. Draw a segment of structure type channel that is orientated in the z-direction. This segment represents one half of the Lumirod. Make sure all tapers are set to none, except for the position taper in the z-direction. This one is set to N/A. The segment reaches the area from the origin to the

coordinate (0,0,L/2) and has a width and height equal to twice the period of the system. (This is to make sure the boundaries of the segment do not intersect with the period of the grating.) The index difference (relative to the background) of this segment is 0.83, hence substitute Rod. Furthermore no energy is absorbed, therefore the imaginary part of the index is set to zero.

To create the other half of the Lumirod, draw the exact same segment as before only now the coordinates are (0,0,-L) to (0,0,0).

The pyramid is the most tricky part of the structure. Draw another channel segment from (0,0,L/2) to (0,0,(L+Period)/2) as before. Since the refractive index of the pyramid structure is 1.936, this time the index difference is set to TiO2. The imaginary part of the index remains zero. Set all tapers equal to zero except for the width and height taper. These will be defined linear. To create a pyramid, define the width and height of the starting vertex equal to the period of the system and set the width and height of the ending vertex to zero. Make sure this device is divided in the number of layers defined in the parameters section. This is necessary for Rigorous coupled wave analysis (section 2.7.3).

To define the periodicity of the system, open the Compute material profile tab. Substitute a domain containing $x \in [-\frac{Period}{2}, \frac{Period}{2}]$, $y \in [-\frac{Period}{2}, \frac{Period}{2}]$ and $z \in [-\frac{L}{2}, \frac{3}{2}L]$. Note that the z-direction of the period has to satisfy that the period ends above the pyramid grating structure and commences in the material of the rod, below the origin.

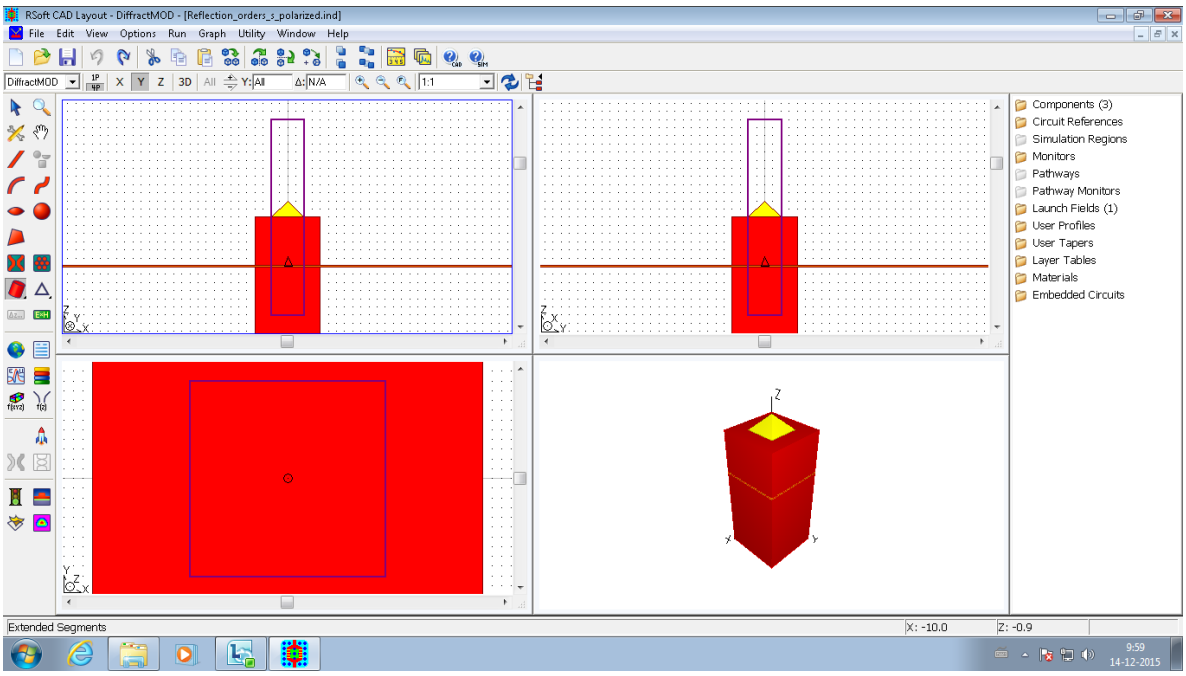

Figure 15: RSoft user interface after setting up the pyramid grating structure and period.

The structure of the model has been prepared. If everything has worked out, the user interface should appear as in figure 15. Now to perform a calculation, we would like to define the polarization of the plane wave and indicate which parameters should be varied. Therefore choose the direction of the polarization in the Plane wave launch options tab and make sure the standard spherical angle convention is applied.
Furthermore define, in the Perform simulation tab, the primary direction in the z-direction and the number of harmonics in both the x-direction and y-direction to be M. For the output we will choose the angle $\phi \in [0, 90]$. (Note that in RSoft ϕ is the polar angle.) Moreover choose the quantity to simulate, for now we will choose the reflection diffraction orders. Save the settings for the calculation, after which we define the other parameter that should be varied in the RSoft most parameters tab. Here we define $\theta \in [0, 90]$. (In RSoft θ is the azimuthal angle.) Since the pyramid grating structure is symmetric over 45° we could have chosen $\theta \in [0, 45]$ to minimize the calculation time. On the measurements tab, select all orders to add them to the calculation and run the simulation.

The calculation time of the simulations with RSoft takes quite some time. On average a simulation run over all relevant angles would take five days for one polarization. Therefore it would be convenient when multiple computers could be linked to each other to calculate through one simulation simultaneously. Moreover it would be extremely useful when the results would be saved while running the calculation so that if a calculation fails at a certain moment, the already obtained results are available.
To make sure a simulation obtains reliable results, parameters describing the model have to be optimized first, hence chosen by hand after varying them in a calculation. This again takes a lot of time, but more important it enlarges the chances of making a mistake by forgetting to optimize and correctly choose a parameter that influences the outcome of the intensities. Inserting this optimization automatically in the calculations of the intensity would prevent making such mistakes.

4 Results

The results in this section are obtained with RSoft. The simulations are modeled as described in section 3.3.1. To give a brief overview of the model, the two dimensional front view of the simulation is shown in figure 16. This figure has already been shown in section 3.
First the results of the Lumirod simulation with a grating period of $d = 500$nm will be discussed, after which the results for the simulation with a 2 micron period will follow.

For both simulations four different calculations have been evaluated. Since we are interested in the s-polarization as well as the p-polarization, both polarization directions are calculated separately by defining the incoming plane wave as a fully s-polarized (or p-polarized) plane wave. Furthermore we simulate all transmission and reflection orders separately for $\phi \in [0, 90°]$ and $\theta \in [0, 90°]$. Since the pyramid structured grating is rotationally symmetric over 90° in the azimuthal angle, we may quadruple the matrices containing the data in such a way that a dataset matrix of all coordinates in space (i.e. $\phi \in [0, 360°]$) is obtained. To this end the matrices are manipulated with a standard coordinate transformation from a cartesian coordinate system to a spherical coordinate system, hence using $\int dxdy = \int \sin(\theta) d\theta d\phi$. (For more details, see the Matlab code in appendix 7.1.1.)
The azimuthal angle is defined as shown in figure 17.

Now a set of matrices describing all diffraction orders separately, in spherical coordinates through the entire space, is accessible. For every diffraction order there is a matrix of which the transmitted intensities are given as the coefficients for every angle of incidence θ and ϕ. The columns correspond to increasing steps of the azimuthal angle $\phi \in (0°, ..., 90°)$ and the rows to steps of the polar angle $\theta \in (0°, ..., 90°)$.

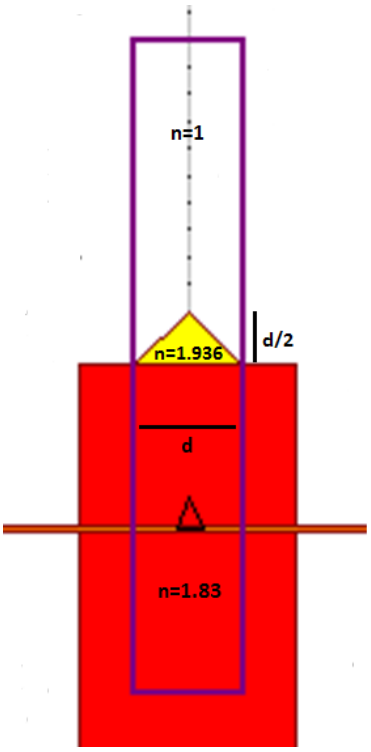

Figure 16: A two dimensional view of one unit cell of the simulated pyramid structured grating, with grating constant d.

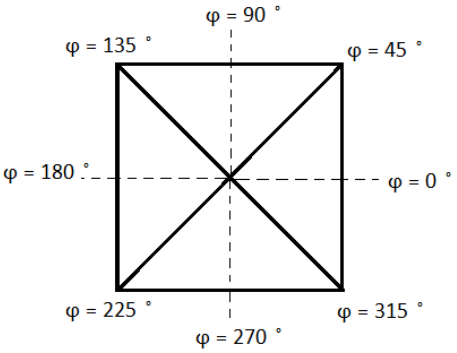

Figure 17: The top view of a pyramid. The angle phi is defined such that $\phi = 45°$ corresponds to a diagonal of the pyramid.

These datasets will be used to calculate the total transmission and total reflection, as a function of the angles of incidence, for both an s-polarized and p-polarized incoming plane wave, by adding up all orders. This calculation is done with Matlab by iteratively adding up the matrices of all diffraction orders of a p-polarized (or s-polarized) plane wave, in a componentwise manner. (See appendix 7.1.2 for the full Matlab code.) Next, only polar angles for which $\theta \in [-57^\circ, 57^\circ]$ holds, will be taken into account. (See the introduction of section 3 for further explanation of this approximation.) We define the vector $\vec{\theta}$ with coordinates $(0^\circ, ..., 90^\circ)$, for which holds that the i^{th} coordinate is

$$\theta_i = \begin{cases} \theta_i & \text{if } \theta_i \in [0^\circ, 57^\circ] \\ \\ 0 & \text{if } \theta_i \in [58^\circ, 90^\circ]. \end{cases}$$

To leave out the data of the matrices for angles $\theta \in [-90^\circ, -57^\circ] \bigcup [57^\circ, 90^\circ]$, we start from the matrices containing the total transmission (or reflection) data in cartesian coordinates. Matrix multiplying these with the vector $\sin(\vec{\theta})$, where the sine acts as an componentwise operator on $\vec{\theta}$, transforms the data to spherical coordinates leaving out the angles $\theta \in [-90^\circ, -57^\circ] \mathbf{U} [57^\circ, 90^\circ]$. Eventually adding up all components of the just calculated vector gives us the total intensity of the matrix for polar angles $\theta \in [-57^\circ, 57^\circ]$. Appendix 7.1.3 contains the Matlab code describing how this calculation is performed.

When we are interested in the total (transmitted or reflected) intensity through the whole space (i.e. $\theta \in [-90^\circ, 90^\circ]$) we add up all diffraction orders and change coordinates to a spherical system, according to appendixes 7.1.2 and 7.1.1 explained earlier this section. The matrix obtained in this way represents the total (s-polarized or p-polarized) transmission or reflection for all angles of incidence through space. Summing over all indices of this intensity matrix, as written in appendix 7.1.4, we obtain the total intensity, I, of the entire space (i.e. an infinite plane).
This calculation corresponds with the formula

$$I = \sum_i \sum_j I_{\theta_i, \phi_j} \sin(\theta_i) \Delta\theta \Delta\phi. \tag{15}$$

Here I_{θ_i, ϕ_j} is the coefficient at place (θ_i, ϕ_j) of the intensity matrix. Note that this coefficient represents the transmission (or reflection) as a function of the angles of incidence in space.
This calculation could also be done by a matrix multiplication with the vector $\sin(\vec{\theta})$ as described before. Instead now $\vec{\theta}$ would be defined $(0^\circ, ..., 90^\circ)$, taking all angles into account.

Finally the total transmission coefficient, T, is calculated

$$T = \frac{T_s + T_p}{2}. \tag{16}$$

Here T_s and T_p represent the total transmission coefficients of a s-polarized and p-polarized incoming plane wave respectively. This implies that T_s is the total transmitted s-polarized intensity from the rod divided by the total s-polarized intensity (i.e. s-polarized reflection and transmission intensity) of the incoming plane wave. The analogous holds for T_p and the reflection coefficients R_s and R_p.

Eventually the gain of the 2μm Lumirod, if compared to an unstructured rod, is calculated. The gain is the ratio between the total transmission coefficient of the Lumirod with a grating structure and an unstructured Lumirod. The total transmission coefficient of an unstructured Lumirod can be approximated theoretically, with the same assumptions made as for the structured Lumirods. Hence for an unstructured rod all light with an angle of incidence $|\theta_{in}| \leq \theta_{crit} \approx 33^\circ$ is, by Snell's law, refracted out of the rod. We will neglect the small Fresnel reflection (figure 10) outside this region. This implies that the intensity of the total transmission of such a rod is proportional to

$$\int_0^{2\pi} d\phi \int_0^{\theta} d\theta' \sin(\theta') = 2\pi(1 - \cos(\theta)) \quad \text{with } \theta = 33^\circ.$$

Since we assume only angles of incidence $|\theta_{in}| \leq 57^\circ$ are present at the end of the rod, the total intensity of the incoming light at the end of the rod is proportional to the same expression above with $\theta = 57^\circ$. Therefore in approximation the theoretically calculated total transmission coefficient of this unstructured rod is

$$\frac{1 - \cos(33^\circ)}{1 - \cos(57^\circ)} = 0.358. \tag{17}$$

4.1 Rod with 500 nanometre pyramid structure

From the obtained datasets multiple figures can be created. To visualize the data in an insightful manner, we prefer a contour plot and a three dimensional surface plot.

Both figure 18 and 19 show the total transmission coefficient of an infinite plane with a pyramid structured diffraction grating and grating constant of 500 nanometre. This total transmission is obtained, from the s-polarized and p-polarized total transmissions, by calculating the total transmission coefficient, for each angle of incidence, according to equation 16.

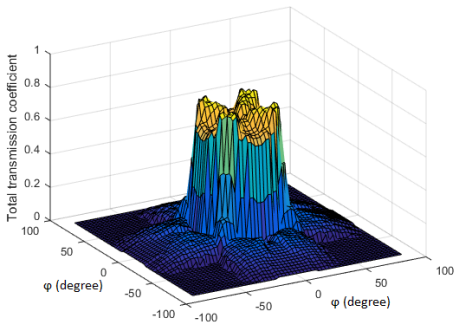

Figure 18: Total transmission coefficient of an infinite plane with a 500nm pyramid structured diffraction grating. The transmission is visualized as a three dimensional polar surface plot in spherical coordinates. The azimuthal angle, ϕ, in the horizontal plane of the coordinate system rotates from 0° to 360°. The polar angle, θ, (the angle with the vertical direction) is an element of the interval [0°, 90°].

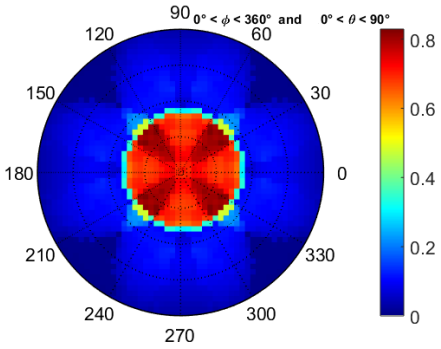

Figure 19: Total transmission coefficient of an infinite plane with a 500nm pyramid structured diffraction grating. The transmission is visualized as a polar contour plot in spherical coordinates. This contour plot corresponds with figure 18. The azimuthal angle, ϕ, rotates from 0° to 360°.

Both figures show that most of the light transmitted initially comes from an angle of incidence $\theta_{in} \in [-\theta_{crit}, \theta_{crit}]$, with $\theta_{crit} = 33°$. The total transmission coefficient within this region is approximately 0.75. Figures 20, 21, 22 and 23 also clearly show this phenomenon.

Figures 20 and 21 show the transmission orders of p-polarized and s-polarized light as a function of θ, at $\phi = 0°$, whereas figures 22 and 23 show the transmission orders of p-polarized and s-polarized light at an azimuthal angle $\phi = 45°$. In all four figures the zeroth, first and second transmission orders are shown.

From these figures it becomes clear that within the region $[-\theta_{crit}, \theta_{crit}]$, the zeroth diffraction order predominates. Hence most of the light transmitted is due to the zeroth order. Outside this region the zeroth order vanishes and only higher diffraction orders contribute to the total transmission. Figures 18 and 19 show that the contribution to the total transmission from all transmission orders outside this region is approximately 0.1. This contribution is mainly due to the first diffraction order as shown in figures 20, 21, 22 and 23.

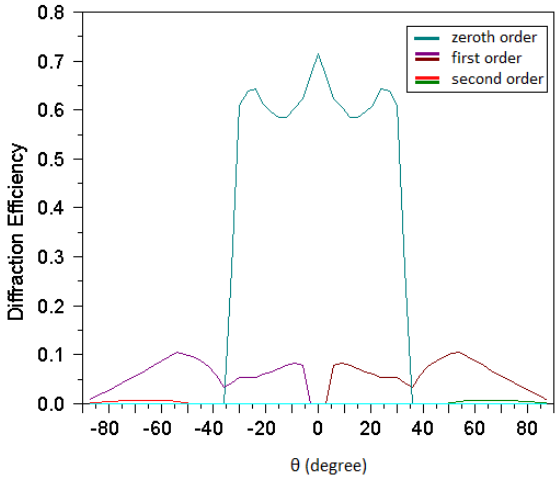

Figure 20: The zeroth, first and second transmission order of p-polarized light on an infinite plane with a 500nm pyramid structured diffraction grating. Here the azimuthal angle of incidence is $\phi = 0°$. Furthermore the polar angle is an element of the interval $[-90°, 90°]$.

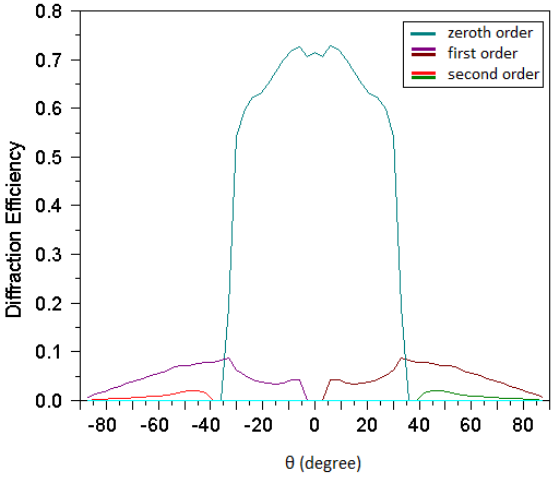

Figure 21: The same as in figure 20 except now for s-polarized light and an azimuthal angle of incidence $\phi = 0°$.

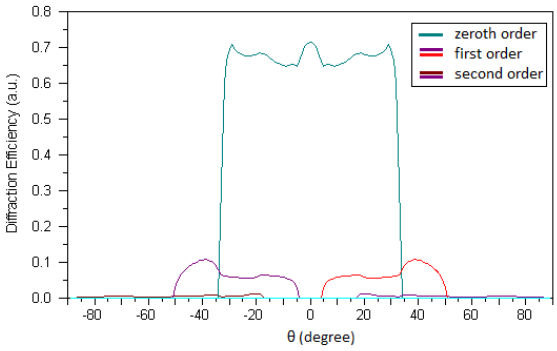

Figure 22: The same as in figure 20 except now for p-polarized light and an azimuthal angle of incidence $\phi = 45°$.

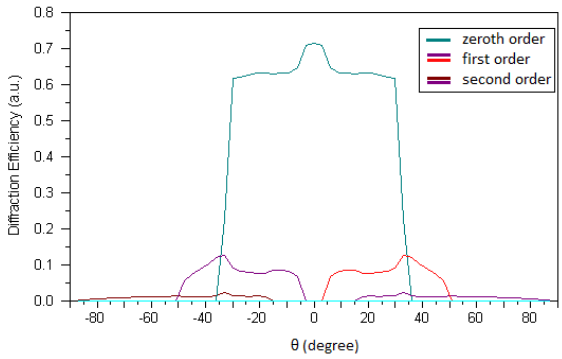

Figure 23: The same as in figure 20 except now for s-polarized light and an azimuthal angle of incidence $\phi = 45°$.

Summing the data of the total s-polarized transmitted intensity over all angles of incidence (equation 15), hence for an infinite plane, and dividing this by the total s-polarized intensity of the incoming plane wave, summed over all angles, we obtain the transmission coefficient of s-polarized light

$$T_s = 0.154.$$

Equivalent, we obtain the transmission coefficient of p-polarized light

$$T_p = 0.153.$$

Next, applying equation 16 results in a total transmission coefficient

$$T = 0.154.$$

Since most light within the Lumirod has an angle of incidence $|\theta_{in}| < 57°$ on the pyramid structured plane, and we approximate this by exclusively taking into account angles for which $-57° < \theta_{in} < 57°$ holds, we will leave out all other angles of θ_{in}, as described previously in this section, and recalculate the transmission coefficients.

We obtain

$$T_s = 0.317$$
$$T_p = 0.307.$$

Hence the "real" total transmission coefficient (meaning the total transmission coefficient that best reflects the Lumirod within the assumptions made (section 3)) is

$$T = 0.312.$$

4.2 Rod with 2 micrometre pyramid structure

Figures 24 and 25 show the total transmission coefficient of an infinite plane with a pyramid structured diffraction grating and grating constant 2 micrometre.

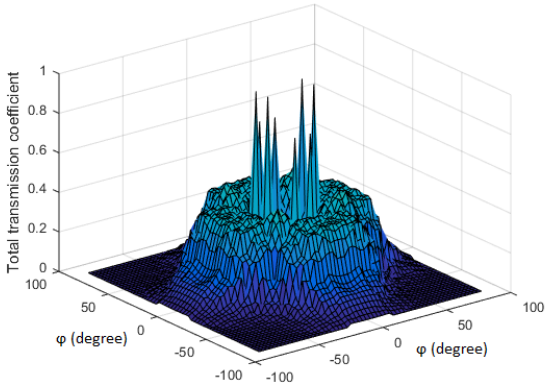

Figure 24: Total transmission coefficient of an infinite plane with a 2μm pyramid structured diffraction grating. The transmission is visualized as a three dimensional polar surface plot in spherical coordinates. The azimuthal angle, ϕ, in the horizontal plane of the coordinate system rotates from 0° to 360°. The polar angle, θ, (the angle with the vertical direction) is an element of the interval $[0^\circ, 90^\circ]$.

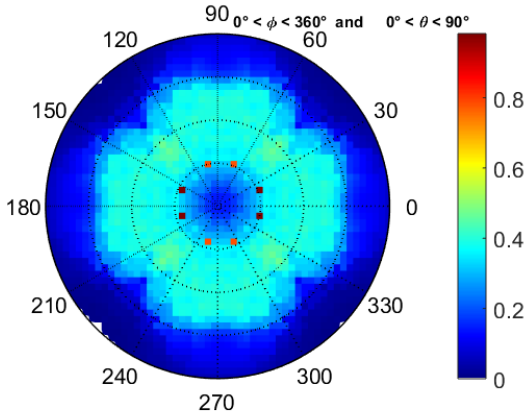

Figure 25: Total transmission coefficient of an infinite plane with a 2μm pyramid structured diffraction grating. The transmission is visualized as a polar contour plot in spherical coordinates. This contour plot corresponds with figure 18. The azimuthal angle, ϕ, rotates from 0° to 360°.

In contrast with the 500nm pyramid structured grating, both figures show that most of the light transmitted comes from an angle of incidence $-50^\circ < \theta_{in} < 50^\circ$. The total transmission coefficient within this region is approximately 0.38. So the transmission for a certain angle of incidence does not reach high values but is spread out over more angles, compared to the 500nm pyramid structure. This phenomena is due to the higher diffraction orders, shown in figures 26, 27, 28 and 29. Here we clearly see that these orders have a large contribution to the total transmission compared to the zeroth order, that at its maximum only contributes 0.04 to the total transmission coefficient. The fact that the higher diffraction orders are of great influence to the total transmission, explains why the total transmission does not vanish for angles of incidence $|\theta in| > \theta crit$.

Again the transmission orders of p-polarized and s-polarized light as a function of θ, at $\phi = 0^\circ$ are shown, this time of the 2μm pyramid structured grating in figures 26 and 27. Whereas figures 28 and 29 show the transmission orders of p-polarized and s-polarized light at an azimuthal angle $\phi = 45^\circ$.

As expected more diffraction orders are observed at the 2μm pyramid structure compared to the two diffraction orders of the 500nm pyramid structured grating.

Note that the eight peaks visible in figures 24 and 25 are not physical since the calculated transmission at these points is larger than one. It is not clear why this result is obtained, but there must have been a bug in RSoft software used to calculate through the simulation. Since these peaks only occur for a couple of angles θ and ϕ they do not have a significant impact on the results. However further research on these peaks would be interesting to find an explanation why the calculation failed for these specific angles.

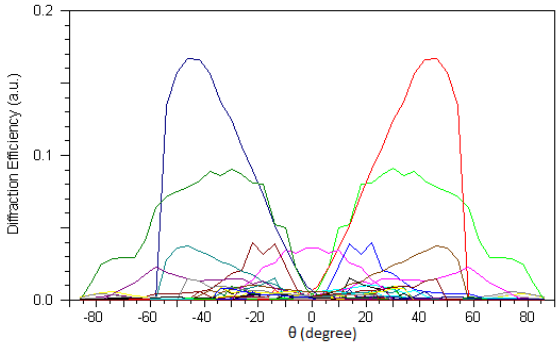

Figure 26: The zeroth to fourteenth transmission order of p-polarized light on an infinite plane with a 2μm pyramid structured diffraction grating. Here the azimuthal angle of incidence is $\phi = 0°$. Furthermore the polar angle is an element of the interval $[-90°, 90°]$.

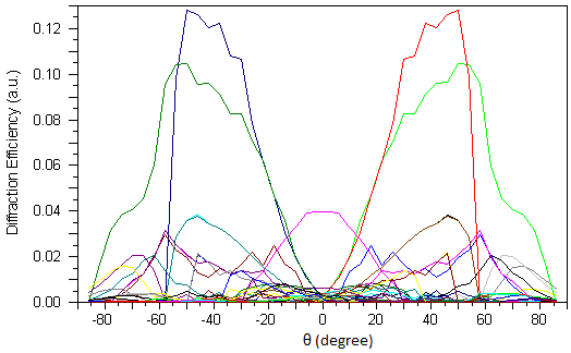

Figure 27: The same as in figure 26 except now for s-polarized light and an azimuthal angle of incidence $\phi = 0°$.

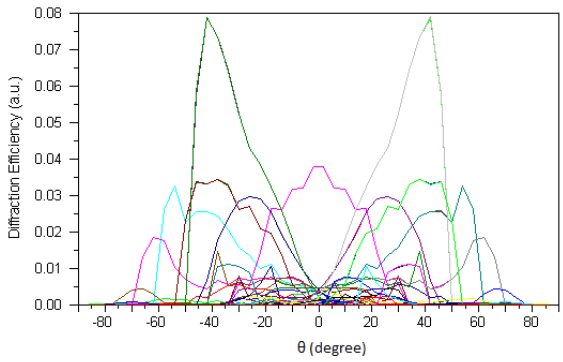

Figure 28: The same as in figure 26 except now for p-polarized light and an azimuthal angle of incidence $\phi = 45°$.

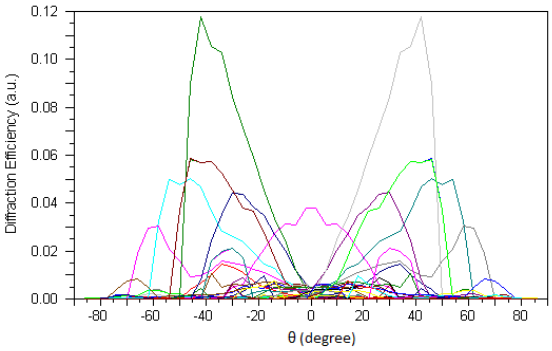

Figure 29: The same as in figure 26 except now for s-polarized light and an azimuthal angle of incidence $\phi = 45°$.

Summing the data of the total s-polarized transmitted intensity over all angles of incidence (equation 15), hence for an infinite plane, and dividing this by the total s-polarized intensity of the incoming plane wave, summed over all angles, we obtain the transmission coefficient of s-polarized light As before, we calculate the total transmission coefficients by summing the data of the transmitted intensity over all angles and dividing this by the total intensity of the incoming wave. Hence we obtain the transmission coefficients:

$$T_s = 0.208$$
$$T_p = 0.173.$$

Applying equation 16, we obtain

$$T = 0.190.$$

Now we are especially interested in transmitted light when taking the boundaries of the rod into account, hence approximating the Lumirod by exclusively using the transmission of the infinite plane of angles for which $\theta \in [-57^\circ, 57^\circ]$ holds. We recalculate the transmission coefficients as described in section 4. In this approximation we obtain

$$T_s = 0.370$$
$$T_p = 0.329.$$

Hence the total transmission coefficient is

$$T = 0.349.$$

These numbers can be compared to those of an unstructured rod. As explained at the end of section 4, the transmission coefficient is in good approximation 0.358. Hence the theoretical gain of this Lumirod, with a pyramid structured grating of period 2μm, height 1μm and refractive index 1.93, is $\frac{0.349}{0.358} = 0.97$. This implies that there is no extraction gain of the 2μm structure with respect to the unstructured rod.
As mentioned in section 1, the experimentally obtained gain of this rod, if compared to a unstructured rod, is within a range 1.55 to 1.74. In comparison with the gain obtained in experiments, this calculated theoretical gain of 0.97 seems rather low.

5 Discussion

If comparing the results of the simulation and the experiment it is striking that the total transmission coefficient of the 2μm pyramid structured grating calculated with the simulations does not match the experimentally obtained fraction of emitted light.
This could be due to the assumption made that exclusively angles of incidence for which $\theta \in [-57°, 57°]$ holds, are taken into account. This assumption to ignore all other angles of incidence has great influence to the transmission coefficient. To illustrate this we will now assume the angle of incidence to be $\theta \in [-51°, 51°]$, which slightly differs from the approximation made in this thesis. Recalculating the total transmission coefficients for the 2μm pyramid grated simulation given this new approximation we obtain:

$$\begin{aligned} T_s &= 0.383 \\ T_p &= 0.344 \\ T &= 0.364. \end{aligned}$$

Hence under this approximation the total transmission coefficient is a factor $\frac{0.364}{0.349} \approx 1.04$ larger.

Several reasons can point out that the assumption, $\theta \in [-57°, 57°]$, might not have been a good approximation for the boundaries of the Lumirod.
First of all we have neglected the fact that light emitted within the Lumirod can immediately reach the structured surface without first reflecting on another surface of the rod. This can cause angles of incidence $|\theta| > 57°$ on the grating structure. Even more we neglected the Fresnel reflection, that can also cause angles of incidence to be larger than we assumed.
Light that scatters from the vertexes and edges of the rod may as well influence the angles of incidence.
It seems to be likely that there is a certain distribution of in which proportions the angles of incidence appear within the Lumirod. This distribution will not be as strict as our assumption that all angles of incidence $|\theta| > 57°$ have probability zero, and all angles $|\theta| \leq 57°$ are equally likely. This could strongly effect the transmission coefficients.

Ray tracing simulations in Philips Research have shown that the real angular distribution extends to higher angles because of skew rays (figure 30). The difference, between the assumption that all angles of incidence $|\theta| < 57°$ are equally likely and the real angular distribution obtained with Ray tracing simulations, is too small to explain the small simulated value for the amount of extracted light.

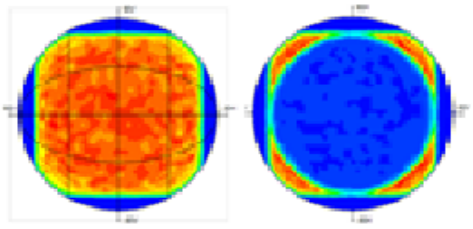

Figure 30: Polar graph of ray tracing simulations show which angles of incidence are present at the end of the Lumirod (left figure). The right figure indicates which angles greater than 57° are present.

Since the s-polarized and the p-polarized transmission coefficient are not the same there could be a dependence of the total transmission coefficient depending on the distribution between these polarizations. It sounds logical to assume the light emitted within the Lumirod can be described as a plane wave of which half of the

light is s-polarized and the other half is p-polarized. However this does not have to be true. Taking the Fresnel reflection into consideration and looking back at figure 10, it is shown that the p-polarized Fresnel reflection is always less than the s-polarized Fresnel reflection. Moreover at one point the p-polarized Fresnel reflection reaches zero, the Brewster angle. Hence it might be that more s-polarized light then p-polarized light remains within the rod.
Since the s-polarized transmission coefficient in the simulation is larger than the p-polarized transmission coefficient, the total transmission coefficient could be higher than we calculated. However, the mentioned ray tracing simulations indicate that the light in the rod nose is essentially unpolarized.

Another reason for the discrepancy between simulation and experiment may be that in the experiment the emitted light includes light reflected from the front surface that, after several reflections to the other rod sides, comes back at the front surface and has another chance to be outcoupled. For an unstructured front surface on a block-shaped rod this is not possible, but it is possible in case of a structured surface. This effect could be quantified by coupling the RSoft simulations to ray-tracing simulations (LightTools). Preliminary LightTools simulations at Philips, using the transmission coefficients found in this work (and a Lambertian approximation for the angular distribution) yields a gain of 1.34, in better agreement with experiment.

Furthermore part of the reason that the theoretically based results do not agree with the experimentally obtained results, done with a Lumirod with a 2μm pyramid structured grating, is probably due to the fact that the 2μm pyramid structured grating is not perfect, meaning it deviates from the geometrical preferred form, while the theoretical model approximates this structure by only deviating from it due to the discretization of computer techniques. The pictures in figure 31 already show a couple of problems that indicate the experimentally created pyramid grated structure shows some deviations. The pyramid structured layer can for instance be torn or the layer is detached from the surface of the Lumirod, hence not the entire surface of the rod is covered with the grating structure. Another important difference between the theoretically simulated geometry and the geometrical form of the experimentally created pyramids is that the pyramids in the experiment are truncated and slightly collapsed, reducing their height (upper picture in figure 3), while the modeled pyramids have perfectly sharp edges and vertexes and a height of half the period. Also the pyramid width may play a role in the difference between the experiment and the simulation. The simulation is modeled with a width of 2μm, while in the experiments the period is 2μm but the pyramids do not exactly connect to their neighbors. There is a small spacing in between the pyramids, meaning the width of the experimentally obtained pyramid grating structure is slightly smaller than 2μm.

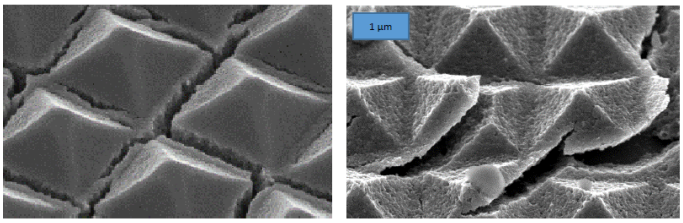

Figure 31: Examples of experimentally created structures on the rod that turned out to have failed [2].

However, also the reference experiments for the unstructured rod may be in error. It was found that the output luminous flux of bare rods may vary by a factor 1.3 or more.

Finally the software to calculate through the modeled simulation could possibly contain bugs, therefore the obtained data with simulating the model could have been incorrect. The eight peaks in figures 24 and 25 are an example of such a bug.

6 Conclusion

The aim of this research is to provide the theoretically calculated transmission of light that diffracts from a Lumirod with a pyramid grating structure (section 1). For a pyramid grating structure of width 2μm and height 1μm we compare these with the experimental results obtained by research group Photonic Materials and Devices of Philips Research.

The light emitted within the Lumirod is approximated by an s-polarized or p-polarized plane wave, diffracting from a pyramid structured grating, described in section 3 and shown in figure 8. The assumption that only angles of incidence $\theta \in [-57^\circ, 57^\circ]$ are present at the grating structure of the rod is made. This is because light reaches the grating by total internal reflection from the sides of the rod.
For a pyramid structured grating with a grating constant of 500nm the s-polarized, p-polarized and total transmission coefficients are obtained

$$\begin{aligned} T_s &= 0.317 \\ T_p &= 0.307 \\ T &= 0.312. \end{aligned}$$

Calculating the s-polarized, p-polarized and total transmission coefficients for the same simulation with instead a period of 2μm, results in

$$\begin{aligned} T_s &= 0.370 \\ T_p &= 0.329 \\ T &= 0.349. \end{aligned}$$

For an unstructured rod, the calculated transmission coefficient is 0.358, slightly more than for the structured case. The experimentally obtained gain for this Lumirod with a pyramid structured grating with grating coefficient 2μm and refractive index 1.936 is within a range 1.55 to 1.74.
The theoretically calculated result of the gain seems rather low compared to these experimentally obtained ratios. This is possibly due to the fact that the Lumirods tested in the experiments do not exactly reflect a "perfect" pyramid structured grating with period 2μm and height 1μm (see section 5 for further explanation). Furthermore, recycling of reflected light would enhance the above mentioned numbers that are based on direct transmission only.

We observe that the calculated transmission coefficient for a simulated Lumirod with period 500nm is less than a Lumirod with period 2μm. Since there are no further results, too little is known to generate a reliable conclusion of which grating structure would optimize the total transmitted light diffracted from the rod. Ongoing research both experimental and theoretical is recommended to analyze why the obtained theoretical and experimental results do not match, as well as which diffraction grating optimizes the total transmission. It is important for this further research to simulate a structure that best reflects the experimentally created grating. Moreover the experimentally obtained gratings should be checked, for instance on whether they cover the entire surface of the Lumirod.

Variations in the grating structure can be made, not limited to the period, height and refractive index of the structure, but also including the shape.

Finally to implement the Lumirod in a LED projector it is requested the light, diffracted from the rod, is transmitted with low angular divergence. Hence research on the diffraction angle would be interesting. One could calculate the diffraction angle for each angle of incidence per order, hereby obtaining the transmission as a function of the escape angle instead of the angle of incidence. This would give insight in whether the transmitted light can be used for projection.

7 Appendix

7.1 Matlab codes

7.1.1 Quadruple

```
function y = viervoudigen(x)

data=transpose(x);
grootte=size(data);
bb=zeros(grootte(2),grootte(2));


step=3;
for i=1:grootte(2);
bb(i,1)=data(1,i);
end
for j=2:grootte(2);
bb(1,j)=data(grootte(1),j);
end
for i=2:grootte(2);
x=i-1;
for j=2:grootte(2);
y=j-1;
polhoek=atan(y/x)*180/pi;
azimuth=sqrt(x^2+y^2);
iazimuth=int16(azimuth)+1;
jpolhoek=int16(polhoek)/step+1;
if iazimuth<grootte(2)+1;
bb(i,j)=data(jpolhoek,iazimuth);
end
end

end
sizebb=size(bb);

bb=transpose(bb);
theta=0:3:3*(sizebb(1)-1);        %theta (rotation angle in the
    plane) is defined here
thetasize=size(theta);
figure(1)
pcolor(theta,theta,bb)
%caxis([0 1])
colorbar

b4=zeros(2*grootte(2)-1,2*grootte(2)-1);
for i=1:grootte(2);
for j=1:grootte(2);
b4(i,j)=bb(grootte(2)+1-i,grootte(2)+1-j);
end
for j=grootte(2)+1:2*grootte(2)-1;
```

```
b4(i,j)=bb(grootte(2)+1-i,j-(grootte(2)-1));
end
end
for i=grootte(2)+1:2*grootte(2)-1;
for j=1:grootte(2)
b4(i,j)=bb(i-(grootte(2)-1),(grootte(2)+1)-j);
end
for j=grootte(2)+1:2*grootte(2)-1;
b4(i,j)=bb(i-(grootte(2)-1),j-(grootte(2)-1));
end
end

%sizeb4=size(b4);
%theta=-3/2*(sizeb4(1)-1):3:3/2*(sizeb4(1)-1);     %theta
    [-87:3:87] (rotation angle in the plane) is defined here
%thetasize=size(theta);
%figure(2)
%pcolor(theta,theta,b4)
%caxis([0 3])
%shading flat
%colorbar



%s = sprintf('57%c', char(176));
%figure(3)
%hold on
%surf(b4)
%title('Graph of angle-filtered data')
%xlabel(['-' s '< \theta <' s]) % x-axis label
%ylabel(['-' s '< \theta <' s]) % y-axis label
%legend('y = sin(x)','y = cos(x)')


y = b4;

end
```

7.1.2 Combining diffraction orders

```
M=16;                              %aantal orders
%string  = 'C:\Users\310209797\Documents\MATLAB\ROD_500nm\
    Transmission_orders_p-polarized_work\results\
    Transmission_orders_p-polarized_dm_de_t_';
%string = 'C:\Users\310209797\Documents\MATLAB\ROD_500nm\
    Transmission_orders_s-polarized_work\results\
    Transmission_orders_s-polarized_dm_de_t_';
%string  = 'C:\Users\310209797\Documents\MATLAB\ROD_500nm\
    Reflection_orders_p-polarized_work\results\Reflection_orders_p-
    polarized_dm_de_r_';
%string  = 'C:\Users\310209797\Documents\MATLAB\ROD_500nm\
    Reflection_orders_s-polarized_work\results\Reflection_orders_s-
```

```
    polarized_dm_de_r_';

%string  = 'C:\Users\310209797\Documents\MATLAB\ROD_2000nm\
    Transmission_orders_p-polarized_work\Transmission_orders_p-
    polarized_dm_de_t_';
%string  = 'C:\Users\310209797\Documents\MATLAB\ROD_2000nm\
    Transmission_orders_s_polarized_work\
    Transmission_orders_s_polarized_dm_de_t_';
%string  = 'C:\Users\310209797\Documents\MATLAB\ROD_2000nm\
    Reflection_orders_p_polarized_work\
    Reflection_orders_p_polarized_dm_de_r_';
string  = 'C:\Users\310209797\Documents\MATLAB\ROD_2000nm\
    Reflection_orders_s_polarized_work\
    Reflection_orders_s_polarized_dm_de_r_';


stringm = [string 'm'];

for i=0:M;
for j=0:M;
if and(i==0, j==0)
data= getdata([string '0_0_vs_phi.dat']);
elseif i==0
data1= getdata([string    num2str(i) '_' num2str(j) '_vs_phi.dat'])
    ;
data2= getdata([string    num2str(i) '_m' num2str(j) '_vs_phi.dat'
    ]);
data = data + data1 + data2;
elseif j==0
data1= getdata([string    num2str(i) '_' num2str(j) '_vs_phi.dat'])
    ;
data2= getdata([stringm   num2str(i) '_' num2str(j) '_vs_phi.dat'])
    ;
data = data + data1 + data2;

else
data1=getdata([string     num2str(i) '_' num2str(j) '_vs_phi.dat'])
    ;
data2=getdata([stringm    num2str(i) '_' num2str(j) '_vs_phi.dat'])
    ;
data3=getdata([string     num2str(i) '_m' num2str(j) '_vs_phi.dat'
    ]);
data4=getdata([stringm    num2str(i) '_m' num2str(j) '_vs_phi.dat'
    ]);
data= data+data1+data2+data3+data4;
end
end
end

dataRs=hoekselectie(data);
```

```
        data=viervoudigen(data);

        %dataTs=data;


        figure(4)
        s = sprintf('90%c', char(176));
        theta = -87:3:87;
        pcolor(theta,theta,data)
        %caxis([0 3])
        shading flat
        colorbar
        %title('Total transmission of a s-polarized plane wave through a
            500nm pyramid structured grating')
        xlabel(['-' s '< \theta < ' s]) % x-axis label
        %ylabel(['-' s '< \theta < ' s]) % y-axis label
        %legend('y = sin(x)','y = cos(x)')

        figure(5)
        surf(theta, theta, data)
        %title('Graph of angle-filtered data')
        xlabel(['-' s '< \theta < ' s]) % x-axis label
        %ylabel(['-' s '< \theta <' s]) % y-axis label
        %legend('y = sin(x)','y = cos(x)')


        %datah=Hoekfilter(data);

        %s = sprintf('57%c', char(176));
        %thetah= -57:3:57;

        %figure(6)
        %pcolor(thetah,thetah,datah)
        %caxis([0 3])
        %shading flat
        %colorbar
        %xlabel(['-' s '< \theta < ' s]) % x-axis label

        %figure(7)
        %surf(thetah,thetah,datah)
        %title('Graph of angle-filtered data')
        %xlabel(['-' s '< \theta <' s]) % x-axis label
        %ylabel(['-' s '< \theta <' s]) % y-axis label
        %legend('y = sin(x)','y = cos(x)')
```

7.1.3 Angle selection

```
function y = hoekselectie(x)
%input must be a not manipulated data matrix of the total intensity (i.e.
    all orders added up)
ruwtransmissionp = transpose(x);
```

```
sintheta=transpose(sin([0:3:87]*pi/180));

for i=21:30          %theta=[0:3:87]  and theta(20)=57degrees so theta(21)
    to theta(30) is 0
sintheta(i,1)=0;
end


M=ruwtransmissionp*sintheta;

totaal = 0;
lengthM = size(M);
for i=1:lengthM(1)                          %summing over all phi
i;
totaal= totaal + M(i,1);
end


y=totaal
```

7.1.4 Adding

```
        % Calculating the total intensity
        transmissionp = viervoudigen(getdata(['C:\Users\310209797\Documents
            \MATLAB\ROD 500nm\Totaal\' '
            Transmission_total_p_polarized_dm_de_t_total_vs_phi.dat']));
        transmissions = viervoudigen(getdata(['C:\Users\310209797\Documents
            \MATLAB\ROD 500nm\Totaal\' '
            Transmission_total_s_polarized_dm_de_t_total_vs_phi.dat']));
        reflectionp = viervoudigen(getdata(['C:\Users\310209797\Documents\
            MATLAB\ROD 500nm\Totaal\' '
            Reflection_total_p_polarized_dm_de_r_total_vs_phi.dat']));
        reflections = viervoudigen(getdata(['C:\Users\310209797\Documents\
            MATLAB\ROD 500nm\Totaal\' '
            Reflection_total_s_polarized_dm_de_r_total_vs_phi.dat']));


        %datatot = reflections + reflectionp +transmissionp + transmissions
            ;

        datatot = dataTs + dataTp + dataRs + dataRp;
        %datatot = dataTp + dataRp;
        %datatot = dataTs + dataRs;


        figure(4)
        surf(datatot)


        lengtht= size(datatot);
```

```
        totaal = 0;

        for i=1:lengtht(1)
        for j=1:lengtht(2)
        totaal= totaal + datatot(i,j);
        end
        end

        totaal



        %Calculating the relevant intensity
        %data = transmissionp + transmissions;
        data = dataTs  + dataTs;



        length= size(data);
        intensiteit = 0;

        for i=1:length(1)
        for j=1:length(2)
        intensiteit= intensiteit + data(i,j);
        end
        end

        intensiteit

        ratio= intensiteit/totaal
```

7.1.5 Read data

```
function y = getdata(x)

fid = fopen(x, 'r') ;              % Open source file.
fgetl(fid) ;                       % Read/discard line.
fgetl(fid) ;                       % Read/discard line.
fgetl(fid) ;                       % Read/discard line.
fgetl(fid) ;                       % Read/discard line.
buffer = fread(fid, Inf) ;         % Read rest of the file.
fclose(fid)

x = x(1:end-4);                    % delete .txt

fid = fopen([x,'','\_new.dat'], 'w')  ;   % Open destination file.
fwrite(fid, buffer) ;                        % Save to file.
fclose(fid) ;

y=importdata([x,'','\_new.dat']);

end
```

7.1.6 Contour figure

```
function Vervolg_figuur(x)
close all
figure(20)
%title('0 < \phi < 360')
%xlabel('0 < \phi < 360') % x-axis label
%hex = data;
hex = x;
LW=1; % linewidth
FS=16  ;% fontsize
thetaticks=[0 20 40 60 80];  % polar plot equidistant in angle with
    0 in the middle,  grid lines at 30, 60, 90
phiticks=[0:30:330];     %  phi labels and grid lines every 30
   degrees


%% plot results
%hex=xlsread('hex')    %% square dataset,  apparently from -80 to +
    80 degrees in 0.5 degree steps
hexrange=80;          %% to avoid white square,  will clip all
   points outside evaluated range (70 deg) to 70 deg.

%% x y coordinates
sizehex=size(hex)
x=-3/2*(sizehex(1)-1):3:3/2*(sizehex(1)-1);
[azimuth yy]=meshgrid(x,x);

%%  clipping
r=sqrt(azimuth.^2+yy.^2);
polhoek=angle(azimuth+1i*yy);
idx=find((r>=hexrange));
azimuth(idx)=hexrange*cos(polhoek(idx));
yy(idx)=hexrange*sin(polhoek(idx));

%% plot
pcolor(azimuth,yy,hex);
axis image;
axis off;
shading flat
colormap jet(256)
a=colormap;
%% white for out of range at lower end of caxis
a(1,:)=[1 1 1];
colormap(a)

%% c-axis range
%caxis([0 3])

%% hide x and y axis
%set(gca,'visible','off')
```

```
hold on

%% over plot polar diagram axis

%% circles at minor ticks
azimuth=[0:0.01:2]*pi;
for q=1:max(size(thetaticks))-1,
r=thetaticks(q);
rc=r*cos(azimuth);
rs=r*sin(azimuth);
plot(rc,rs,'k:','LineWidth',LW)
end

%% outside circle not dotted
r=thetaticks(q+1);
rc=r*cos(azimuth);
rs=r*sin(azimuth);
plot(rc,rs,'k','LineWidth',LW)

%% radial lines at fixed phi
r=[0:0.1:max(thetaticks)];
rmax=max(thetaticks);

for q=1:max(size(phiticks)),
plot(r*cos(phiticks(q)*pi/180),r*sin(phiticks(q)*pi/180),'k:','
    LineWidth',LW)
text(rmax*1.13*cos(phiticks(q)*pi/180),rmax*1.13*sin(phiticks(q)*pi
    /180),num2str(phiticks(q)),'FontSize',FS,'HorizontalAlignment','
    center','VerticalAlignment','middle')
end

%% make a bit of space on the right so the zero does not fall
    behind the colorbar
xlim([-rmax,1.3*rmax]);

%% colorbar
colorbar('fontsize',FS);

s=sprintf('0%c', char(176));
l=sprintf('360%c', char(176));
n=sprintf('90%c', char(176));
title([' ' s ' < \phi < ' l ' and -' n ' < \theta < ' n])
end
```

References

[1] Dick K. G. de Boer, Dominique Bruls and Henri J. B. Jagt, *High-brightness source based on luminescent concentration*. Technical note Philips Research, Eindhoven, first volume, 2015.

[2] Anne E. J. Souren, Dick K. G. de Boer, Henri Jagt, Marc A. Verschuuren and Remco van Brakel, *Improved brightness luminescent concentrating source by high refractive index micro-patterns*. Technical note Philips Research, Eindhoven, first volume, 2015.

[3] https://en.wikipedia.org/wiki/Maxwell%27s_equations

[4] David J. Griffiths, *Introduction to Electrodynamics*. Pearson, Harlow, fourth edition, 2014.

[5] Max Born & Emil Wolf, *Principles of optics*. Pergamon Press, Oxford, sixth edition, 1986.

[6] https://en.wikipedia.org/wiki/Magnetic_field

[7] https://en.wikipedia.org/wiki/Permittivity

[8] https://en.wikipedia.org/wiki/Permeability_(electromagnetism)

[9] https://en.wikipedia.org/wiki/Fresnel_equations

[10] https://en.wikipedia.org/wiki/Crystal_momentum

[11] https://en.wikipedia.org/wiki/Spherical_coordinate_system

[12] https://en.wikipedia.org/wiki/Reciprocal_lattice

[13] David L. Sidebottom, *Fundamentals of condensed matter and crystalline physics*. Cambridge University Press, New York, first edition, 2012.

[14] https://en.wikipedia.org/wiki/Lattice_constant

[15] https://en.wikipedia.org/wiki/Orthorhombic_crystal_system

[16] https://en.wikipedia.org/wiki/Snell%27s_law

[17] https://en.wikipedia.org/wiki/Bragg%27s_law

[18] https://en.wikipedia.org/wiki/Floquet_theory

[19] http://math.arizona.edu/ dwang/FloquetTheory.pdf

[20] http://www.emba.uvm.edu/ jxyang/teaching/Floquet_theory_Ward.pdf

[21] http://www.jirka.org/diffyqs/htmlver/diffyqsse23.html

[22] Brian C. Hall, *Lie Groups, Lie Algebras, and Representations: An Elementary Introduction*. Springer, New York, first edition, 2003.

[23] John B. Schneider, *Understanding the Finite-Difference Time-Domain Method*. first edition, 2015.

[24] https://en.wikipedia.org/wiki/Finite_element_method

[25] Jian-Ming Jin, *Theory and Computation of Electromagnetic Fields*. John Wiley & Sons, New Jersey, first edition, 2010.

[26] https://en.wikipedia.org/wiki/Rigorous_coupled-wave_analysis

[27] John J. Hench & Zdenek Strakos, *The RCWA method- a case study with open questions and perspectives of algebraic computations*. Electronic Transactions on Numerical Analysis, Kent State University, volume 31, 2008. .